Politechnika Krakowska
im. Tadeusza Kościuszki

Katedra Technologii Informatycznych
w Inżynierii (L-10)
Wydział Inżynierii Lądowej

KTIwI

Degree Program: Civil Engineering
Project area: Computer Modeling

PRACA DYPLOMOWA INŻYNIERSKA

Bachelor of Science

FINITE ELEMENT MODELING OF AN ALUMINUM ALLOY WITH LARGE STRAIN THERMO-ELASTO-PLASTICITY

MODELOWANIE SKOŃCZENIE ELEMENTOWE STOPU ALUMINIUM ZA POMOCĄ TERMO-SPRĘŻYSTO-PLASTYCZNOŚCI Z UWZGLĘDNIENIEM DUŻYCH ODKSZTAŁCEŃ

by

Agnieszka Sobierańska

Project Advisor: PhD Eng. Balbina Wcisło

Grade: ……..……

Advisor's signature: ……..

Date: ……..

Kraków, January 2025

Contents

Chapter 1

Introduction

Thermoelasticity and thermoplasticity are essential concepts in the continuum mechanics of materials, describing the correlation between thermal and mechanical properties of materials. Understanding this reciprocation is fundamental to accurately predict the behavior of materials vastly used in engineering. This thesis focuses on an extensive analysis of the thermo-mechanical behavior of Aluminum Alloy 5083, with particular emphasis on the coupled phenomena of thermo-elastic cooling and thermo-plastic heating.

The analyzed model takes into account thermal expansion, dependence of material's parameters on the reference temperature and the influence of deformations on the material's conductivity, based on the Fourier's law further discussed in Subsection 2.4.4. The model allows for simulations regarding deformations of samples in a large range of temperature as well as large strain deformations due to the fact that small deformations are not assumed - the model provides geometrical nonlinearity. The tests are supplemented by convection simulations to better imitate true physical conditions during real-life testing of the samples.

By employing numerical models, specifically AceGen and AceFEM, we can conduct a detailed analysis of thermo-elastic cooling in the elastic range, and heating during the process of plastic yielding. The thermo-mechanical analysis is rooted in the formulation of the Helmholtz free energy, which is a fundamental thermodynamic potential governing the material's response, which is also analyzed and exhibited in the following work.

The notion of large strain deformations is described at length in several publications among which is (Bonet and Wood, 2008).

The research presented in the work is outlined in the subsequent order. Chapter 2 is dedicated to the formulation of fundamental thermodynamic laws and physical quantities implemented in used models. In Chapter 3, author inspects and reports test results for the thermo-elastic range. Sequentially, Chapter 4 presents the thermo-elasto-plastic model. The thesis closes Chapter 5 inclusive of final remarks.

Chapter 2

Foundational concepts

2.1 Kinematics

The detailed description of the notion of kinematics applied in the examined case can be found e.g. in (Bonet and Wood, 2008). A general motion of a deformable continuous body can be analyzed in the initial configuration denoted by the vector $\mathbf{X}$ at time $t = 0$. Particles of the deformable body in the current configuration are described with the vector $\mathbf{x}$ at a time $= t$. The motion can be described by a mathematical mapping joining reference and current configuration as follows

$$\mathbf{x} = (\mathbf{X}, t). \tag{2.1}$$

Deformation gradient is defined in a standard way

$$\mathbf{F} = \frac{\partial \boldsymbol{\varphi}(\mathbf{X}, t)}{\partial \mathbf{X}}, \qquad J = \det(\mathbf{F}). \tag{2.2}$$

where the function $\boldsymbol{\varphi}$ describes movement of the body such that $\mathbf{x} = \boldsymbol{\varphi}(\mathbf{X}, t)$. Such definition implies that initial and current configurations can be compared without knowledge of the intermediary configurations (Ĉanadija and Brnić, 2004). To differentiate the thermo-elastic and plastic deformation, the following form of the deformation gradient is presented:

$$\mathbf{F} = \mathbf{F}^r \mathbf{F}^p, \tag{2.3}$$

where $\mathbf{F}^r$ and $\mathbf{F}^p$ stand for reversible thermoelastic deformation and plastic deformation, respectively. Decomposition of the deformation gradient for the finite elasto-plasticity was introduced in (Lee and Liu, 1968) and was widely used among posterior scientists. An uncoupled form of the reversible part of Eq. (2.3) was proposed by (Stojanović et al., 1964) and is presented in a form

$$\mathbf{F}^r = \mathbf{F}^\theta \mathbf{F}^e, \tag{2.4}$$

where $\mathbf{F}^\theta$ refers to deformation resulting from thermal expansion and $\mathbf{F}^e$ refers to the elastic contribution. Finally, Eq. (2.2) and Eq. (2.3) can be expressed in the following form

$$\mathbf{F} = \mathbf{F}^\theta \mathbf{F}^e \mathbf{F}^p = \mathbf{F}^\theta \mathbf{F}^m, \tag{2.5}$$

where $\mathbf{F}^m$ stands for the deformation gradient of a mechanical character. The thermal part $\mathbf{F}^\theta$ is assumed to be volumetric, hence

$$\mathbf{F}^\theta = (J^\theta)^{\frac{1}{3}} \mathbf{I}, \qquad J^\theta = \det(\mathbf{F}^\theta), \tag{2.6}$$

where $\mathbf{I}$ is the second-order identity tensor. Deformation caused by thermal changes is then denoted as

$$J^{\theta} = e^{3\alpha_T(T-T_0)}, \tag{2.7}$$

further explained in (Lu and Pister, 1975). In Eq. (2.7) the absolute temperature is denoted by T, T_0 denotes the reference temperature, and α_T is the coefficient of linear thermal expansion.

The decomposition presented in Eq. (2.5) and Eq. (2.7) is then a basis to presenting the mechanical part of the Eq. (2.5) as

$$\mathbf{F}^m = e^{-\alpha_T(T-T_0)}\mathbf{F}. \tag{2.8}$$

2.2 Helmholtz free energy

The Helmholtz free energy is a critical thermodynamic quantity that finds extensive application in modeling and simulating material behavior under various conditions. Introduction of the general free energy form is given in spacial configuration In the following section, three models for the Helmholtz free energy are tested using a single finite element.

$$\psi = \theta(T) + M(J,T) + U(J,T) + W(\bar{\mathbf{b}}^r, T) + K(\alpha, T), \tag{2.9}$$

where

$$\bar{\mathbf{b}}^r = \det(\mathbf{b}^r)^{-1/3}\mathbf{b}^r \tag{2.10}$$

and α is an internal variable related to hardening.

In the following section, three models for the Helmholtz free energy are tested using a single finite element. The author tested three different variants of the volumetric part of the Helmholtz free energy. In this work there are three ways of formulation and implementation of the Helmholtz free energy in order to select a formula most accurate to the model. The objective is to investigate the influence of the adopted free energy form on the mechanical and thermal material response. The tests for different variants are being performed for thermo-elasticity with fixed material's parameters.

Following the initial comparison, we select the most promising model and proceed to simulate a more complex structure: an aluminum plate. This phase involves using three different mesh densities to understand the model's performance in capturing the nuances of material behavior at varying levels of discretization.

Depending on the model used, the components of Eq. (2.9) are going to differ. Detailed description of all components of Eq. (2.9) can be found simplified in Subsection 3.3.

2.3 Heat transfer

Engineers, physicists and scientists all over the world distinguish three main ways of heat transfer. The fundamental ones are: conduction, convection and radiation. There is also another crucial way of heat transfer connected to fluid mechanics and earth sciences called advection, but this matter will not be a subject of this work. For more information about advection the author refers the reader to such works as (Mohamed and Paleologos, 2018) or (Sun and Zhang, 2020).

2.3.1 Conduction

Thermal conductivity, usually represented by k is a measure of the material's ability to transfer heat. Expressed in [W/mK] or [J/sKm], allows the heat to transfer through materials of higher k value, rather

than those of low thermal conductivity. The term thermal conductivity should not be used interchangeably with the term thermal conduction.

Thermal conduction is the diffusion of heat within one material or between two bodies in contact. It is defined as the heat transferred some distance l between the two temperatures per unit of time t. The heat exchange occurs via contact of molecules of higher temperature with colder particles. Warmer particles carry more kinetic energy, therefore they collide with the rest of the particles, evening out the temperature lever throughout the body or transferring it to another object.

When a material has a higher thermal conductivity value, the process of heat transfer will be much faster than in cases when dealing with materials of low thermal conductivity coefficient, which is precisely why e.g. building materials used for thermal insulation like mineral wool or expanded polystyrene (EPS) have low thermal conductivity coefficient k also commonly expressed as λ. In the table below, Table 2.1 the author presents values of thermal conductivity k of the most common building and structural materials.

Material	Value [J/(sKm)]
Aluminum AW5083	121
Steel	50
Concrete	3
Glass	1
Plaster	0.8
Porotherm brick	0.12
Wood	0.12
Mineral wool	0.04

Table 2.1: Thermal conductivity coefficients for the most common building materials.

In civil engineering there are two fundamental ways for the thermal conduction to take place. The first one is steady-state conduction. Steady-state conduction happens, when the rate at which the heat transfers remains constant. The second most common kind is transient heat conduction. A conduction when the heat passing through a body keeps fluctuating, and by that, is not constant is called a transient heat conduction process (Bahrami, 2011).

2.3.2 Convection

Next to radiation and conduction we can also distinguish a phenomenon of convection. Most common in liquids and gases, convection happens when particles holding more heat energy take place of the particles holding less heat energy. Important to know is that such definition of convection applies exclusively in the context of thermodynamics. Convection is a very efficient way of heat transfer because it maintains a steep temperature gradient between the body and surrounding air or water (Sokolova, 2019). The rate of heat transfer through convection depends on the temperature difference between the hot and cold regions. A larger temperature difference will lead to more intense convection, which can further amplify the thermal stresses and reactions (Incropera et al., 2007).

One can distinguish two types of convective heat transfer. That being free, also known as natural convection, and forced convection. Free convection can take place due to the laws of physics. The movement of gas or a liquid is caused by the differences in the density of areas of different temperature. Due to the Archimedes's principle the gas or liquid having higher temperature and less density starts to rise. On its way it encounters colder areas of higher density, which makes the exchange of the energy to the latter one possible. Forced convection happens when the movement of gas or liquid is induced by the work of e.g. ventilator or a fan. Heat transfer rate can be calculated according to the formula

$$\dot{Q} = hA\Delta T, \tag{2.11}$$

where $\dot{Q}$ stands for rate of heat transfer per unit time, h represents convection heat-transfer coefficient, A is the exposed surface area and ΔT is the temperature difference.

Convection is influenced by numerous factors. Among many others time plays a significant role in the analysis of the convection phenomenon. The longer the time of the experiment, the temperature will be more homogeneous, which has been tested and proven and results of such simulation are analyzed later in this work. A very significant role in the analysis of the convection process is material's physical ability to transfer heat. Although the process of convection is not directly dependent on the material's properties, those do have a great influence on the outcome of the experiment.

Another crucial factor influencing heat exchange by convection is a quantity called convection coefficient. Convection coefficient oppositely to the property discussed before, does not describe material. The convection coefficient, often called the heat transfer coefficient, denoted in literature by h_{conv} or h describes the conditions present during the heat transfer. The general definition of the convection coefficient is

$$h_{conv} = \frac{q_n}{\Delta T}, \tag{2.12}$$

where q_n denotes heat flux, and ΔT represents the difference in temperatures between the surface of the sample and the surrounding environment. The range of values of h_{conv} used for convection calculations varies widely dependent on the conditions assigned for the test. Depending on the direction of air flow and position of the plate, the results will differ. In Table 2.2 the author presents ranges of h_{conv} coefficient appropriate for different convection conditions (ResearchGate, nd), (EngineersEdge, nd). A broad-spectrum study on convection phenomenon was conducted in the University of Technology in Torno (Chiavazzo et al., 2014). Another significant work on this matter is (Churchill and Chu, 1975) which states about, among others, equations for laminar and turbulent free convection for a vertical plate.

Type of convection	Variety	Range [J/(sKm^2)]
Free	Horizontal surface	5 - 25
	Vertical surface	10 - 100
Forced	Laminar flow	10 - 100
	Turbulent flow	100 - 1000

Table 2.2: Convection coefficients for air.

The process of convection is also heavily influenced by the roughness of the surface of the material and shape of the sample. The rougher the surface, the more turbulence of air or liquid will occur, increasing the rate of heat transfer. The shape of the sample can also have an impact on the rate of convection happening by affecting the flow patterns. Although there is no direct association of the shape or dimensions of the sample with the general convection occurrence, the results will vary when applying a plate 2 mm thick like in our case, and a plate 100 mm thick. In case of the thinner plate, convection will influence the results significantly due to the fact, that e.g. elastic heating or cooling will be getting balanced by the convection happening on the surface. In case of the thicker plate, the sample will be so thick, that convection occurring on the surface will not affect the results as much, which is also proven in this work.

As trivial as the case might seem, the process of heat transfer by convection is also dependent on the temperature. When the temperature of a sample increases, a decrease in density is observed, for proof of such behavior the author refers the reader to Fig. 2.1 and Fig. 3.18.

The results of computer simulations taking into account heat transfer by convection can be found in this work in Subsection 3.5.

2.3.3 Radiation

The third mentioned in this work way of heat transfer is radiation. Along with conduction and convection, radiation is an another fundamental way of heat transfer, which in this work will be shortly discussed to complete the heat transfer description, but it will not be taken into account in simulations.

Thermal radiation is emitted by all bodies with temperature greater than 0 K. Emissivity is strictly a material's property commonly denoted with ϵ. It is not related to specific radiation conditions. Some radiation-related terms are: transmission (τ), absorption (α) and reflection (ρ). There is a strong relationship between them and is represented by the equation below (Incropera et al., 2017):

$$\tau + \alpha + \rho = 1 \tag{2.13}$$

The Eq. (2.13) states, that the sum of all transmitted, absorbed and reflected radiation must be equal to the total incident radiation. Incident radiation here is understood as the total electromagnetic radiation that is able to reach given surface. Under the term electromagnetic radiation the author understands various forms such as light, heat or other types of energy waves. The notion of incident radiation is discussed in detail in (Holman and Churchill, 1999).

Most emission surrounding us in everyday life is invisible to the human eye, but a special equipment e.g. an infrared camera is capable to capture such emission. Emission of thermal radiation becomes visible to human eye in high temperatures estimated at above 525°C, the glow that becomes then visible is called incandescence. The heat that travels from Sun to Earth through space can be transferred because thermal radiation is possible. A black body is called a radiating body which is in equilibrium with its surface, and the surface of the body has a property to absorb all incident electromagnetic radiation. A black body is also considered to be the perfect emitter. Such emission from the perfect emitter is called black-body radiation. The emissivity of a radiating body is explained as the ratio between its emission relative to emission of a black body. As a results of that notion, a black body has an emissivity of $\epsilon = 1$. The distribution of black-body radiation is in detail described in the cutting-edge paper (Planck, 1901) where the German scientist also introduced the Planck's law. In the mentioned work one can also find in-depth clarification of the whole radiation notion.

Below the reader can find a table presenting emissivity for various commonly used building and finishing materials. Note, that given values are given as ranges due to the fact, that exact values can vary depending on the roughness of the finishing surface, weathering, moisture content, oxidation and other factors.

Material	Range [-]
Aluminum AW5083 (polished)	0.03 - 0.08
Steel (polished)	0.05 - 0.10
Concrete	0.70 - 0.90
Glass (clear)	0.90 - 0.95
Plaster	0.70 - 0.90
Porotherm brick (unpainted)	0.70 - 0.90
Wood (unpainted)	0.80 - 0.95
Mineral wool	0.90 - 0.95

Table 2.3: Emissivity values for the most common building materials.

As one can see from Table 2.3 emissivity is an unitless quantity. More in-depth assessment of thermal emissivity values for the common building materials are elaborated in (Albatici et al., 2013).

Material's emissivity is an important quality in civil engineering because of a number of reasons. One

of many parameters influenced by material's emissivity factor is building energy efficiency. When dealing with materials of higher emissivity, heat losses are greater also making the cost of living or working greater, than in case of using low emissivity materials. That is why as a designer one should opt for e.g. thermal insulation materials with the lowest possible values of ϵ.

Another phenomenon influenced by the value of emissivity, strongly connected to the first one is thermal comfort. By thermal comfort the author understands the state of satisfaction or dissatisfaction with thermal conditions of the user of a given space (Humphreys and Parsons, 2002). Thermal comfort is one of top priorities for HVAC (heating, ventilation, and air conditioning) design engineers and will not be further discussed in this work.

2.4 Thermo-mechanical coupling

2.4.1 Thermal expansion

Thermal expansion is an increase or decrease of the body's size, as a result of change in temperature. It is possible for such a phenomenon to happen due to increased speed of movement between molecules inside the body, which makes them move further apart from one another (Roberts and Kirkwood, 1940). Thermal expansion coefficient is commonly denoted by α_T and can be expressed as a function of temperature. Such measure was taken in this work.

The coefficient of linear thermal expansion α_T can be defined by the following equation

$$\alpha_T = \frac{\Delta L}{L \Delta T}, \tag{2.14}$$

where ΔL is the change in length, L is the initial length of the sample and ΔT is the change in temperature.

Table 2.4 presents thermal expansion coefficients for the most common building materials.

Material	Value [1/K]
Aluminum AW5083	2.3e-5
Steel	1.2e-5
Concrete	1e-5
Glass	9e-6
Plaster	8e-6
Porotherm 25 brick	7e-6
Wood	5e-6
Mineral wool	2e-5

Table 2.4: Thermal expansion coefficients for most common building materials.

In civil engineering the amount of linear thermal expansion of elements like e.g. rods has a significant impact on strain. The strain resulted from thermal expansion can be defined as

$$\epsilon_{thermal} = \alpha_T \Delta T, \tag{2.15}$$

where $\Delta T = (T - T_0)$.

2.4.2 Thermo-elastic coupling - Gough-Joule effect

The Gough-Joule effect was mostly researched and studied for elastomers like rubber. If a rubber band is subjected to stretching action, and then heated, the band will contract, rather than expand further. Such

phenomenon was first observed by John Gough at the very beginning of the XIXth century, and then later, in the 1850s investigated more by James Joule (Gough, 1805).

Despite the fact that the Gough-Joule effect was discovered and examined for elastomers, there are a few sources describing the phenomenon for metals. One of such is (Holzapfel, 2000). In his book he states that 'Polymers are entropic' and 'Metals are energetic', which means, that they manifest the properties shown in Table 2.5. The Gough-Joule effect is taken into account in the model for which the simulations are being held. For an aluminum, which by the given classification, is an energetic material, the Gough-Joule effect is showing by the cooling of the sample in the range of elastic deformations.

Polymers	Metals
Entropic	Energetic
Total stress is entirely caused by a change in entropy with deformation	Entropy does not change with deformation at all
Internal energy does not change with deformation	Internal energy changes rapidly with deformation
A piece of rubber warms up when stretching	An elastic spring of metal cools down when stretching
A rubber band under constant tension will substantially shrink upon heating and expand upon cooling	An elastic metallic spring under constant tensile force will expand upon heating and shrink upon cooling
Elasticity arises through entropic straightening of a polymer chain, followed by recoiling into a conformation of maximum entropy	Elasticity emerges due to distance changes between atoms against atomic attractive forces, which then restore the material to its initial state after deformations - substantial volume changes accompany deformations

Table 2.5: Comparison of polymers and metals in terms of behavior upon stretching (Holzapfel, 2000).

2.4.3 Plastic dissipation

Energy dissipation in elastoplastic solids and structures is the result of an irreversible dissipative process in which energy is transformed from one form to another and entropy is produced (Yang et al., 2017). Plastic dissipation takes place because of the irreversible deformations of the elastoplastic materials.

Scientists and engineers all around the world researched the plastic dissipation phenomenon for many years to better understand its effect on structures and foundations. Early publications on energy dissipation are e.g. (Farren and Taylor, 1925) and (Taylor and Quinney, 1934). Both works focus on the process of converting mechanical work into heat during plastic deformation of metals, but the latter one concentrates on metals undergoing plastic deformation due to cold working. The authors of publications cited above presented results of experiments and proved that majority of the input mechanical energy is converted to heat, but the remaining, significantly smaller part is proven to be deposited form of cold work energy. A coefficient called Quinney-Taylor coefficient was introduced in more recent works, usually denoted by β. β describes the ratio of plastic work converted into heating and ranges between 0.6 and 1.0 (Clifton et al., 1984), (Belytschko et al., 1991).

2.4.4 Fourier's law

It is a fact that heat transfer takes place when the molecules move more rapidly when their temperature rises. The molecules collide, transmitting their energy to adjacent molecules. This process abides by the Fourier's law.

When discussing heat transfer, Newton's law of cooling is considered as a physical law, usually taking place as a consequence of the Fourier's law. Newton's law of cooling is actually a discrete and electrical analog of the Fourier's law (Incropera et al., 2007). The differential form of the Fourier's law for the isotropic material, also known as the law of heat conduction, can be written as

$$\mathbf{q} = -k\nabla T, \tag{2.16}$$

where $\mathbf{q}$ is the local heat flux density, k stands for the considered material's conductivity and ∇T is the temperature gradient. The Fourier's law states that the rate of heat transfer through a material is proportional to the negative gradient in the temperature and to the area, at right angles to that gradient, through which the heat flows (Incropera et al., 2007). Another source presenting an alternative formulation of the heat transfer is (Çengel and Ghajar, 2014). This book discusses Fourier's law as part of the fundamental principles of conductive heat transfer.

2.4.5 Temperature dependent material parameters

Table 2.6 presents generalized material properties of Aluminum Alloy 5083 at room temperature. Further in this section, diagrams presenting selected material properties depending on temperature are presented.

Property	Symbol	Value	Unit
Modulus of elasticity	E	7.0e10	N/m^2
Bulk modulus	K	7.6e10	N/m^2
Shear modulus	G	2.6e10	N/m^2
Initial yield stress	σ_{y0}	2.8e8	N/m^2
Residual yield stress	$\sigma_{y\infty}$	3.5e8	N/m^2
Hardening modulus	H	2e9	N/m^2
Saturation constant	δ	19.618	-
Density	ρ	2662	kg/m^3
Conductivity	k	121.9	J/(sKm)
Heat capacity	c	916.7	J/(kgK)
Thermal expansion coefficient	α_T	2.3e-5	1/K
Thermal softening modulus	H_T	0.0016	1/K

Table 2.6: Material parameters.

Temperature	Conductivity (W/m °C)	Specific heat (J/kg °C)	Density (kg/m^3)
−20	112.5	924.1	2673.9
80	122.7	984.2	2642.7
180	131.6	1039.6	2629.4
280	142.3	1081.2	2611.5
380	152.5	1136.6	2589.3
480	159.5	1178.2	2567
580	177.2	1261.4	2549.2

Figure 2.1: Temperature dependent properties of AA5083 (Elsayed et al., 2017).

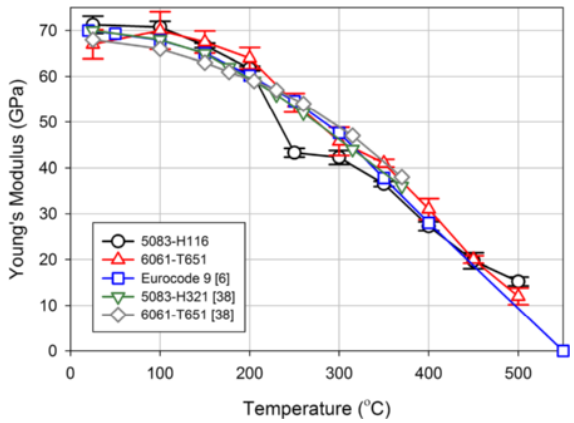

Figure 2.2: Young's modulus vs. temperature (Summers et al., 2015).

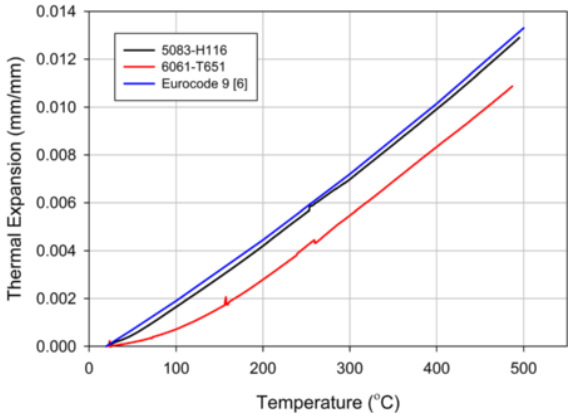

Figure 2.3: Thermal expansion coefficient vs. temperature (Summers et al., 2015).

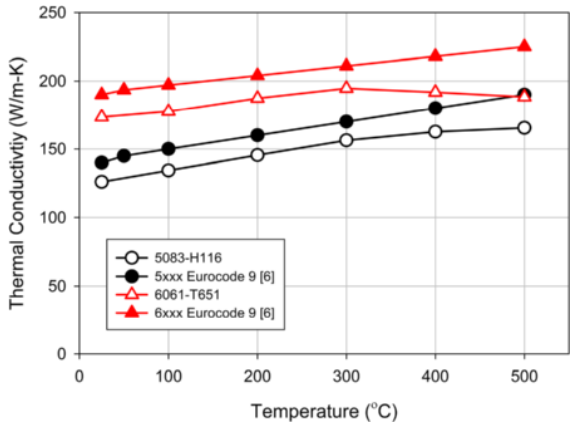

Figure 2.4: Heat conductivity vs. temperature (Summers et al., 2015).

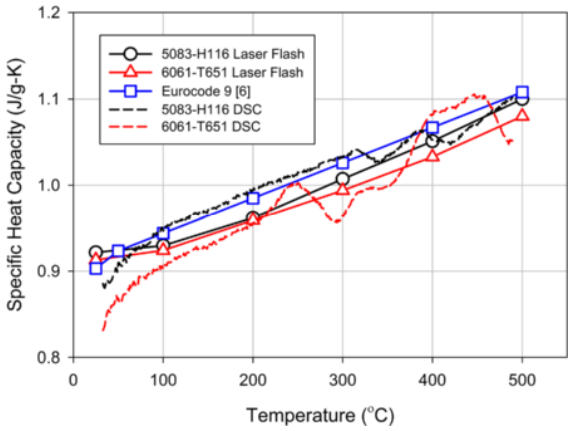

Figure 2.5: Specific heat vs. temperature (Summers et al., 2015).

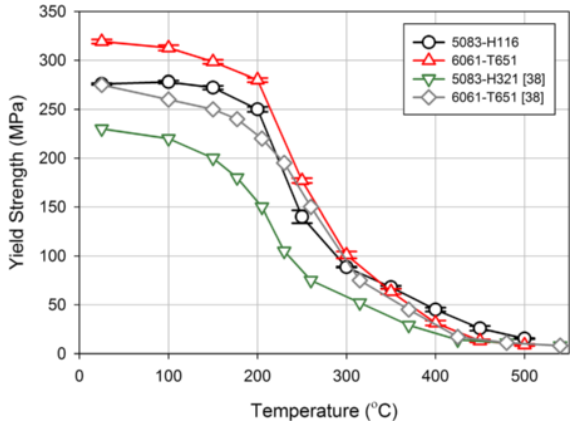

Figure 2.6: Yield strength vs. temperature (Summers et al., 2015).

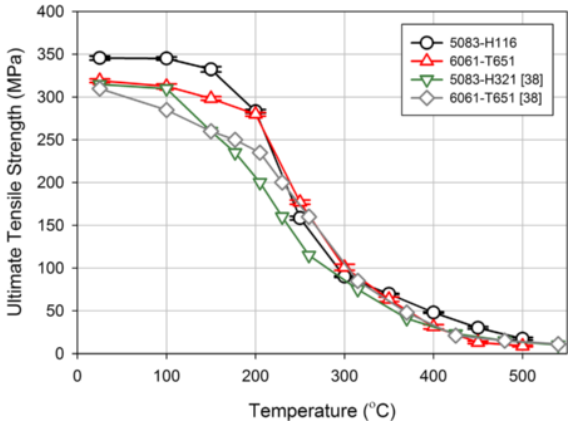

Figure 2.7: Ultimate tensile strength vs. temperature (Summers et al., 2015).

Further information regarding mechanical and thermal properties of Aluminum Alloy 5083 and similar, can be found in (Summers et al., 2015). Information regarding the material's change in density with temperature can be found in (Elsayed et al., 2017) in the table from Fig. 2.1.

The source (Summers et al., 2015) also provides with a diagram showing a relationship between engineering stress [MPa] and logarithmic strain [-] depending on the reference temperature.

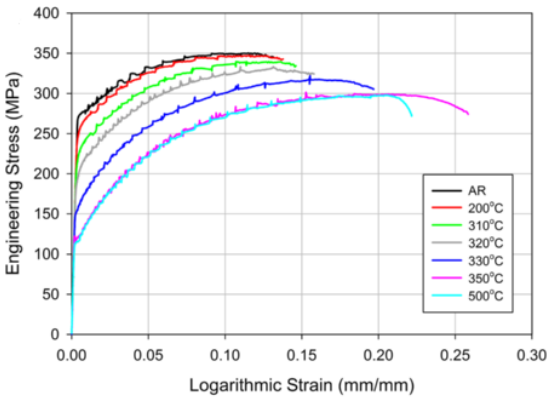

Figure 2.8: Engineering stress vs. logarithmic strain (Summers et al., 2015).

Chapter 3

Thermo-elasticity

3.1 Description of the Thermoelastic Model

Thermoelastic model accounts for two governing equations needed to be solved. The first equation is the balance of linear momentum which can be derived on the basis of the Helmholtz energy (Korelc and Wriggers, 2016). The specific forms of the free energy are given in Subsection 3.3.

The second equation is the balance of energy

$$c_0\dot{T} = \mathrm{Div}(\mathbf{Q}) - H \tag{3.1}$$

where c is heat capacity, $\dot{T}$ is temperature rate, $\mathbf{Q}$ - Piola-Kirchhoff heat flux, symbol Div is divergence in reference configuration and H is heat source due to thermal coupling.

$$H = T\frac{\partial^2\psi}{\partial\mathbf{F}\partial T} : \dot{\mathbf{F}} \tag{3.2}$$

The rate of temperature and deformation gradient are calculated in the algorithm using backward Euler scheme.

As it was mentioned in Subsection 2.4.4 isotropic Fourier's law is defined in the current configuration for the Kirchhoff heat flux density vector $\hat{\mathbf{q}}$ (Haupt, 2002)

$$\hat{\mathbf{q}} = -k\mathrm{grad}(T) \tag{3.3}$$

and for the equation written above the following relation holds between $\hat{\mathbf{q}}$ and $\mathbf{Q}$

$$\mathbf{Q} = -k\mathbf{C}^{-1}\mathrm{Grad}(T) \tag{3.4}$$

where $\mathbf{C} = \mathbf{F}^T\mathbf{F}$, k is conductivity and $\mathrm{Grad}(T)$ is gradient of the temperature in reference configuration.

3.2 Description of simulations

The model used in thermoelastic analysis is simulated using the finite element method (FEM). Because the thermoelastic problem is a coupled problem, which means that it involves an interaction between two or more physical phenomena, the implementation of the finite element method is performed by the means of advanced software technology, i.e. Wolfram Mathematica packages AceGen and AceFEM, incorporating such solutions as automatic differentiation (AD), symbolic and algebraic systems and problem solving environments (Korelc, 2009). The cited work contains detailed description of the automation of transient coupled problems.

Numerical simulations of thermoelasticity include three analyzed aspects. The first one being tests for different free energy functions, in particular different volumetric parts. Firstly one cubic FE is being

subjected to tension, secondly a rectangular plate is subjected to non-uniform tension - analysis for different meshes and elongation rate. Tests for temperature dependent material parameters are the second objective of numerical simulations of thermoelasticity. One cubic finite element is tested for the influence of implementing temperature dependent material parameters, as well as tension at different reference temperature. The last objective of thermoelastic simulations are tests for different thermal boundary conditions. A thin plate with constant material parameters is under uniform tension, and thermal boundary conditions change to either insulation or convection.

Material parameters are taken from Table 2.6.

If not stated otherwise, the insulation is assumed for thermal boundary conditions.

3.3 Analysis of different potentials

3.3.1 Models

In this Section the attention is paid to numerical comparison of results for different Helmholtz free energy Eq. (2.9). For thermoelastic material hardening $K(\alpha, T)$ is absent. Terms $\theta(T)$ and $W(\bar{\mathbf{b}}^r, T)$ are assumed in the forms

$$\theta(T) = c\left((T - T_0) - T\ln\frac{T}{T_0}\right) \tag{3.5}$$

$$W(\bar{\mathbf{b}}^r, T) = \frac{G}{2}\left(\mathrm{tr}(\bar{\mathbf{b}}^r) - 3\right) \tag{3.6}$$

Three forms of $U(J, T)$ are considered and present below. Following (Simo and Miehe, 1992) the part of the free energy related to thermal expansion, i.e. $M(J, T)$, is related to the volumetric part according to formula

$$M = -3\alpha_T(T - T_0)\frac{\partial U}{\partial J} \tag{3.7}$$

thus the choice of $U(J, T)$ influences not only volumetric response of the material, but also thermal expansion and thermo-elastic coupling.

Model 1

In the first model we have implemented the free energy form further described in (Ristinmaa et al., 2007). The following forms of the volumetric part of free energy and the internal energy function associated with the thermal expansion, respectfully, are implemented

$$U(J) = \frac{1}{2}\kappa(\ln(J))^2 \tag{3.8}$$

$$M(J) = -3\alpha_T(T - T_0)\kappa\frac{\ln(J)}{J} \tag{3.9}$$

Model 2

In the second model we have implemented the free energy form described further in the article (Miehe, 1995). The forms of functions U and M are used

$$U(J) = \kappa((J - \ln(J) - 1) \tag{3.10}$$

$$M(J) = -3\alpha_T(T - T_0)\kappa\left(1 - \frac{1}{J}\right) \tag{3.11}$$

Model 3

In the third model the free energy form described in the article (Ĉanadija and Brnić, 2004) is implemented in the following forms

$$U(J) = \frac{1}{2}\kappa\left(\frac{1}{2}(J^2-1) - \ln(J)\right) \tag{3.12}$$

$$M(J) = -3\alpha_T(T-T_0)\frac{1}{2}\kappa\left(J - \frac{1}{J}\right) \tag{3.13}$$

3.3.2 Comparison of models - results for 1FE

Calculations were performed for one finite element (FE). The element has the following dimensions: $L = 10$ mm, $W = 10$ mm and $H = 10$ mm. A visual, three dimensional (3D) representation of the element can be found in Fig. 3.1. The element is elongated to $\Delta L = \frac{L}{200}$ in time $t = 10$ s. Boundary conditions allow for free deformation in transverse directions.

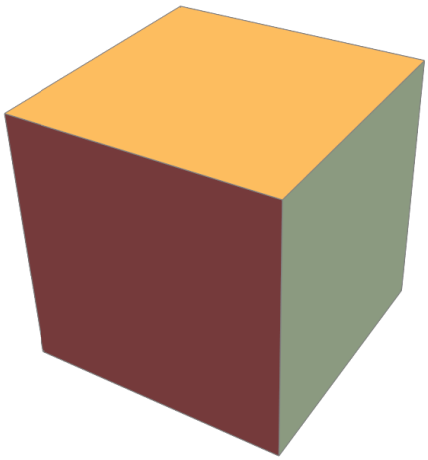

Figure 3.1: Visual representation of 1FE in 3D space.

The results from the simulation are presented in Fig. 3.2 and Fig. 3.3. By dint of conducting the simulation, it became possible to determine, that the type of the applied model, does, in fact influence the results. One can clearly see, that in case of the first, and last model, the reduction of temperature was more significant, than in case of the second model. From Fig. 3.2 Model 1 and Model 3 appear to give the same results, but after closer examination of the numerical results, there is a slight difference on the fourth decimal place. The type of the model used in the simulation does not influence the values of reactions for the finite element, which can be seen in Fig. 3.3.

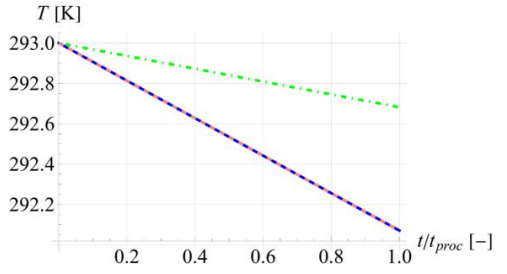

Figure 3.2: Change in temperature.

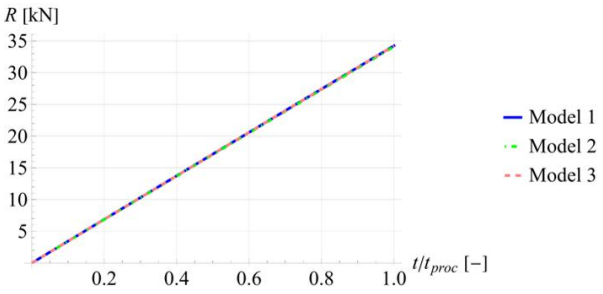

Figure 3.3: Change in magnitude of reactions.

3.3.3 Results for Model 1 for elongated plate

In this subsection results and conclusions for aluminum plate tests are being analyzed. An aluminum plate of an alloy 5083, with the following dimensions was analyzed: $L = 100$ mm, $W = 50$ mm and $H = 10$ mm. In Fig. 3.4 the author presents a visual representation of the plate.

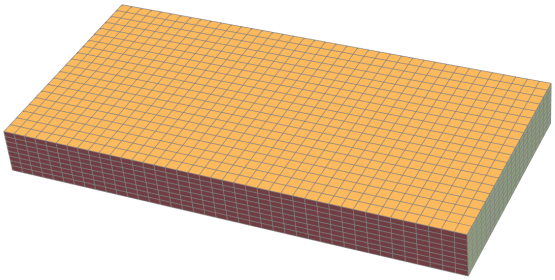

Figure 3.4: Visual representation of the aluminum plate with the finest mesh.

The plate was subjected to elongation by $\frac{L}{150}$ within 10 sec. In this test the plate's sides perpendicular to the tension direction are restrained, thus the non-uniform deformation is obtained shown in Fig. 3.5.

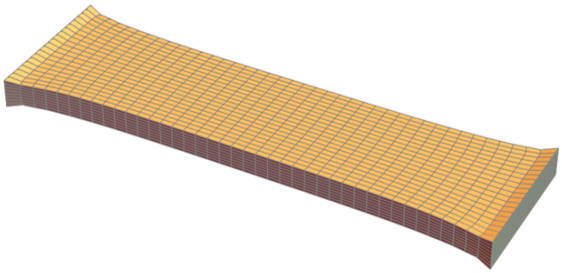

Figure 3.5: Visual representation of the deformed aluminum plate.

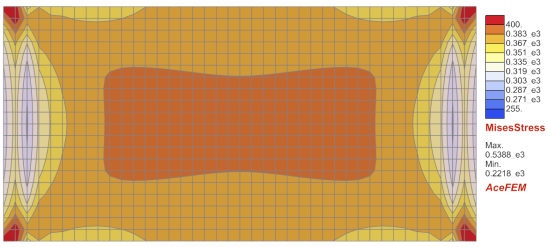

Figure 3.6: Mises stress distribution at the end of the test.

As one can see in Fig. 3.6, the biggest concentration of Mises stresses presents near the clasps and in the center of the sample. The results vary from 538.8 MPa to 221.8 MPa. With such stresses for the given material, the elastoplastic behavior is observed, which means, that the sample entered yielding stage and another model should be applied for further tests. In the subsequent sections of this thesis a presentation and interpretation of a more advanced model considering plastic behavior of the material can be found. Such model can be freely used for considered simulations, owing to the fact, that it represents real behavior of the sample. In Fig. 3.7 the author presents distribution of temperature in the sample at the end of the process which lasts 10 s. The time in which the test was carried out was relatively long, which made the homogeneous distribution of temperature possible. On the contrary, in Fig. 3.8 the author presents the temperature distribution after the test lasting only 0.1 s which proves, that in shorter time duration of the test, the temperature distribution is not homogeneous.

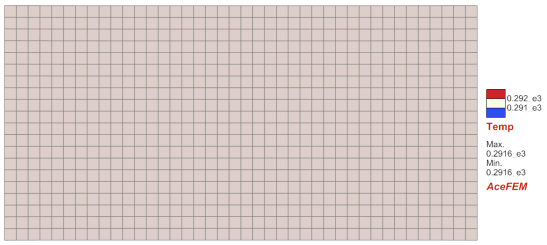

Figure 3.7: Temperature distribution after the test of duration 10 s.

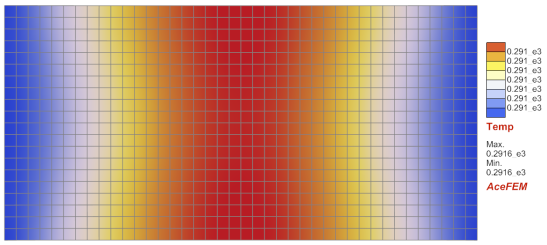

Figure 3.8: Temperature distribution after the test of duration 0.1 s.

In the figures below, one can see the change of temperature in the midpoint of the sample, and on the second figure the author presents the change in the magnitude of reactions, respectively.

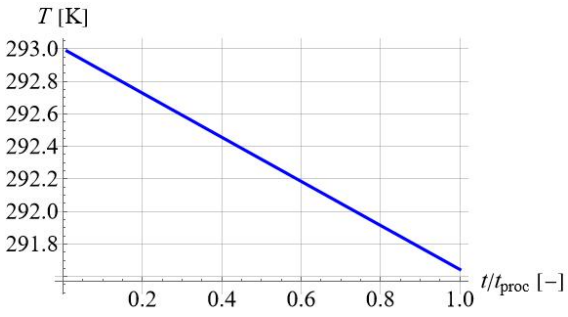

Figure 3.9: Change in temperature in the mid point of the sample.

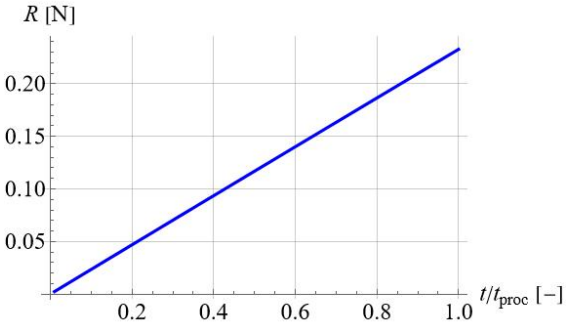

Figure 3.10: Change in the magnitude of reactions in the mid point of the sample.

Meshes

Three meshes were implemented, and the simulation of an aluminum plate was conducted for each of them. The simulations were conducted using the free energy form described in Model 1, which presents with larger difference in temperature, than Model 2.

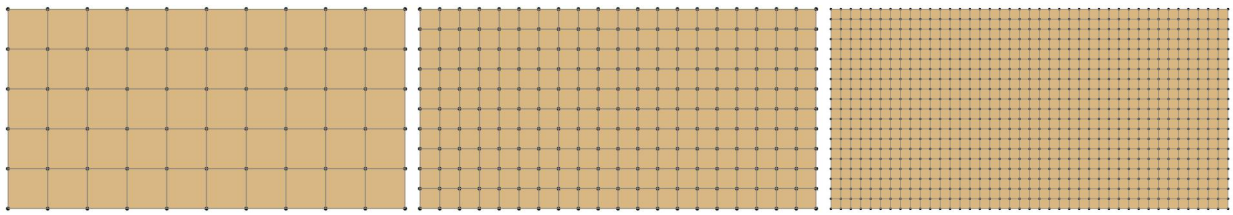

(a) Coarse mesh. (b) Medium mesh. (c) Fine mesh.

Figure 3.11: Visual representation of different mesh refinement used in the test.

Mesh 1 refers to Fig. 3.11a, Mesh 2 is a medium refinement mesh seen in Fig. 3.11b and Mesh 3 is the finest mesh seen in Fig. 3.11c.

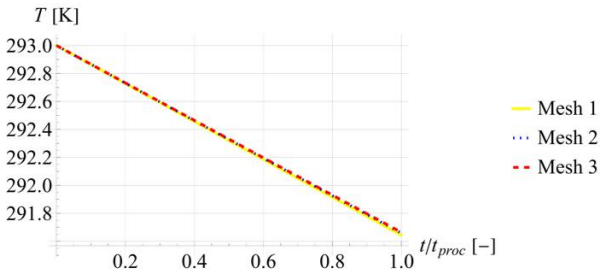

Figure 3.12: Influence of density of mesh on the temperature.

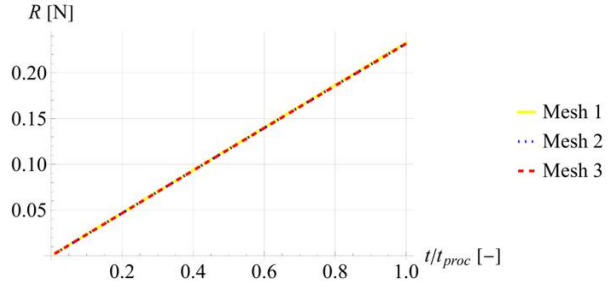

Figure 3.13: Influence of density of mesh on the reactions.

From Fig. 3.12 we can see, that the density of mesh influences the final results of the temperature difference, however the influence, is very slight. Though, from Fig. 3.13 we can see, that the density of mesh does not influence the final results of the reactions.

3.4 AA5083 mechanical and thermal parameters approximations

An appropriate linear, quadratic, third order and logistic sigmoidal approximation was conducted based on results from experimental tests from Fig. 2.2 - 2.7. The results of approximation are shown in Figs. 3.14 - 3.20.

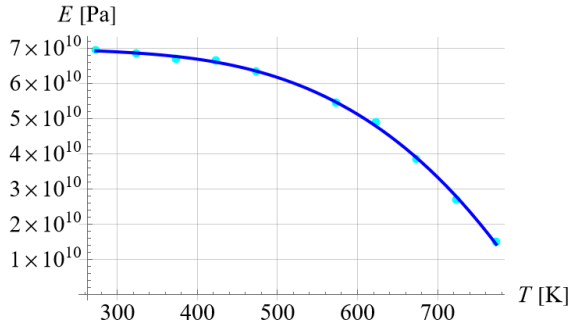

Figure 3.14: Approximation of the Young's modulus vs. temperature.

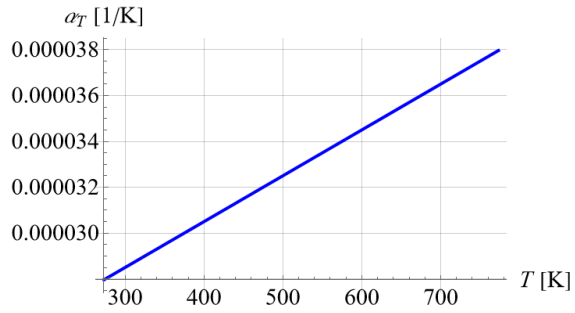

Figure 3.15: Approximation of the thermal expansion vs. temperature.

Fig. 3.15 presents approximation of the thermal expansion property of Aluminum Alloy 5083. Fig. 2.3 provides us with experimental data for AA5083-H116, AA6061-T651 and also the data according to (CEN, 2005). European norm (CEN, 2002) provides us with a formula for ϵ in the following form

$$\epsilon = \frac{\Delta l}{l}, \tag{3.14}$$

where l is the length of the sample at 20°C. For temperature T ranging from 0°C to 500°C the following function of ϵ was implemented

$$\epsilon(T) = 0.1 \times 10^{-7} T^2 + 22.5 \times 10^{-6} T - 4.5 \times 10^{-4}, \tag{3.15}$$

then later a derivative of ϵ with respect to T was derived to receive the following form of thermal expansion α_T

$$\alpha_T(T) = 0.0000225 + 2 \times 10^{-8} T. \tag{3.16}$$

The author applied the function provided by the (CEN, 2002) for the approximation of the thermal expansion property function to reduce the magnitude of error.

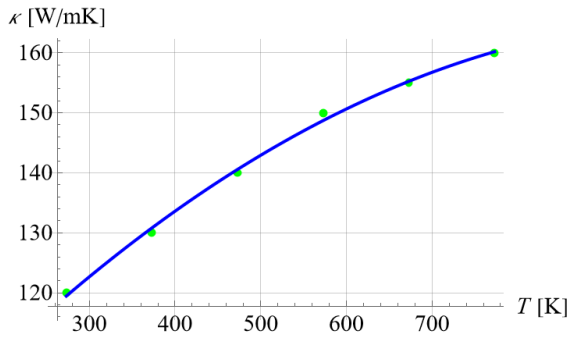

Figure 3.16: Approximation of the thermal conductivity vs. temperature.

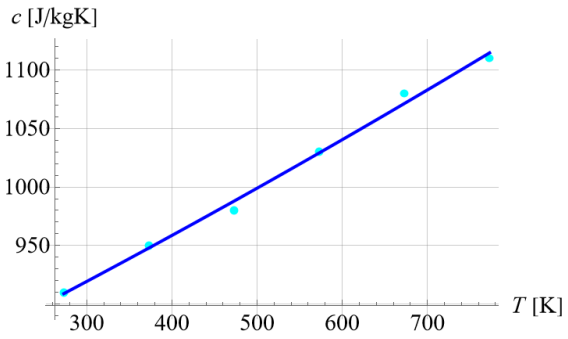

Figure 3.17: Approximation of the specific heat capacity vs. temperature.

The experimental data given in the table from Fig. 2.1 was also approximated using linear function and the result is shown in Fig. 3.18.

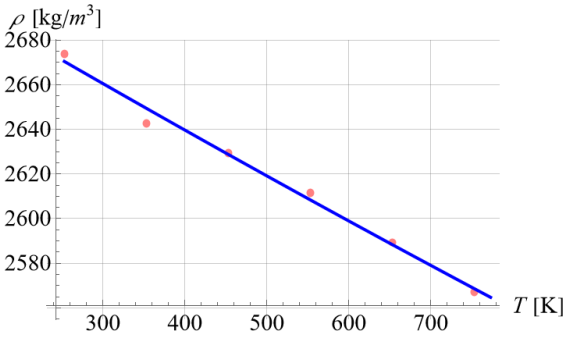

Figure 3.18: Approximation of the Density to Temperature function.

The following two graphs presenting approximation of the yield strength σ_{y0} with respect to temperature T and ultimate tensile strength $\sigma_{y\infty}$ with respect to temperature T were approximated with application of different tools to obtain the best fit. The author presents trials of approximation of the functions from Fig. 2.6 and Fig. 2.7 along with the final approximation on the figures below.

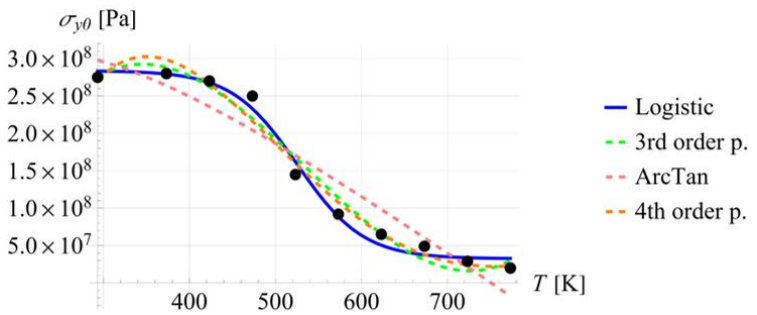

Figure 3.19: Approximation of the yield strength vs. temperature.

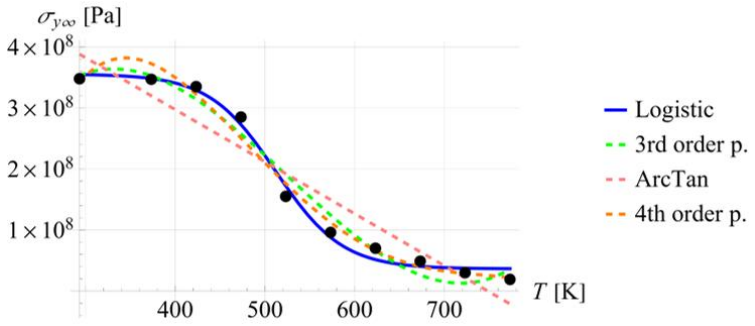

Figure 3.20: Approximation of the ultimate tensile strength vs. temperature.

Firstly, the approach was to approximate the σ_{y0} and $\sigma_{y\infty}$ as a function of T by means of the third order polynomial approximation. As one can see on both, Fig. 3.19 and Fig. 3.20, the third order polynomial approximation could be accepted, but only in the range between 293.15 K and approximately 615 K. In higher temperatures the approximation first underestimates the real properties of the sample, and then begins to overestimate them at the very end. The second approach was to approximate the mentioned functions applying the arctan approximation. Such an idea was not acceptable because of very low degree of accuracy. Thirdly, a fourth order polynomial approximation was subjected to the test, but again the results could not be accepted. While in higher temperature conditions the function behaves well, and gives high degree of accuracy, at lower temperatures, the function heavily overestimates the material's abilities, therefore this solution also could not be accepted. Lastly, the author applied a logistic sigmoid function approximation, which provides enough accuracy that the results can be accepted. The formula for logistic sigmoid function used by the author for the approximation purposes has the following form

$$f(x) = a + \frac{d-a}{1+e^{-b(x-c)}}, \tag{3.17}$$

where a is the lower asymptote of the function, b controls the steepness or growth rate of the sigmoid curve, c is the midpoint, or the value of x where the function reaches the halfway point between a and d, and d is the upper asymptote. The algorithm of acquiring the correct position and form of approximation by means of the logistic sigmoid function was a challenge for the author, which was tackled by application of artificial intelligence (AI) tools. The AI tool was asked to estimate initial a, b, c and d parameters, which were later introduced into the Matlab code, which calculated final, more accurate parameters. The parameters given as a solution of Matlab code calculations were then applied to the code made for approximation purposes in the Wolfram Mathematica software to achieve a graphical result coherent with the rest of the figures. It is important to note, that the results are valid for AA5083-H116 alloy, which has higher tensile stress resistance comparing with e.g. AA5083-H111 due to the strengthening processes the material undergoes.

After conducting approximation of material's parameters to temperature functions introduced in this work in Subsection 2.4.5, two tests of one finite element in tension were created to check if the Model is going to behave differently with implementation of two different codes. The reader can find an in-depth description of the Model in this work in Subsection 3.3. In the first code, the results of the approximation were included in the code as functions with variable T_0, here equal to 293.15 K. The second code was prepared with already calculated values of material's parameters and included in the code as constant parameters. For simplification of captions, the author refers to the results obtained from two codes as Code 1 and Code 2 respectively. In Figs. 3.21 and 3.22 one can see a comparison of change in temperature in time, as well as change in magnitude of reaction depending on which code was applied.

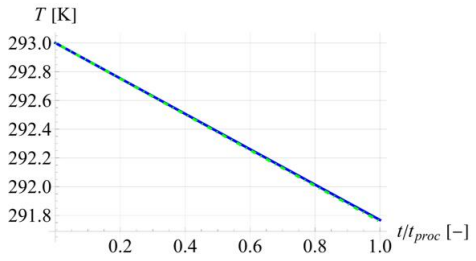

Figure 3.21: Dependence of change in temperature on the type of code applied

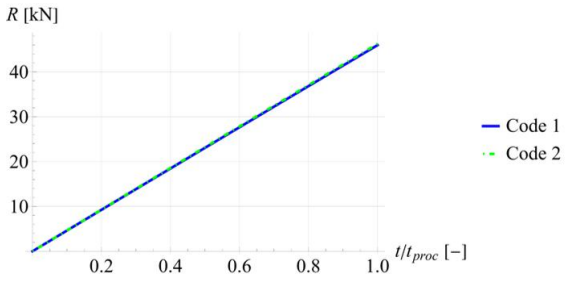

Figure 3.22: Dependence of change in reaction on the type of code applied

As expected, the temperature graphs vary slightly depending on the selected code. The code with constant material parameters presents with marginally greater temperature difference, than in case of the code with functions representing relationship between material's parameters with temperature implemented. The same behavior was observed in the change of reactions throughout the test. In case of Code 1 change in the magnitude of reactions was observed to be faintly smaller than in case of Code 2 result.

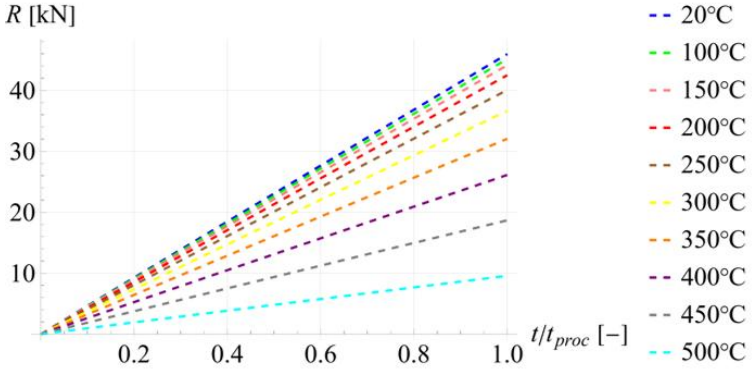

Figure 3.23: Dependence of reactions on reference temperature.

Depending on the value of reference temperature, the magnitude of reactions throughout the test will be different. Such behavior was proven by the results of the test, which is visible in Fig. 3.23. As expected, the value of reactions increases with time. Reference temperatures were given here in Celsius degrees as it should be more transparent for the reader. The higher the reference temperature, the final magnitude of reactions lowers significantly. An important behavior to note is the tendency of the magnitude of reactions to change in nonlinear manner rather than linear when the temperature rises.

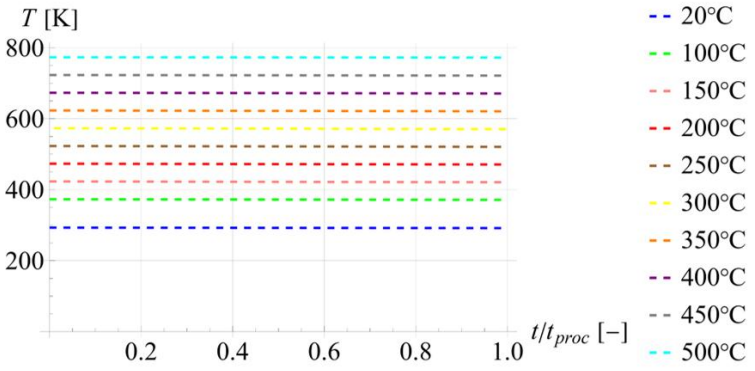

Figure 3.24: Dependence of change in temperature on reference temperature.

A comparison of how the temperature is going to change starting from various reference temperatures

was also performed. The differences are too small to be noticed in Fig.3.24, but in Fig. 3.25 one can find results showing how the temperature changes depending on the initial temperature. Another comparison can be seen in Fig. 3.26. The author compared graphs for the same reference temperatures as in previous figures in the manner $T - T_0$, where T is temperature at the end of the test, and T_0 is the initial temperature.

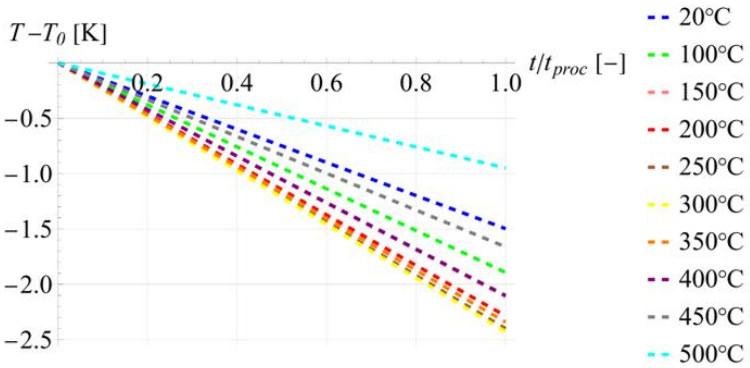

Figure 3.25: Dependence of difference between final and initial temperature vs. reference temperature.

Fig. 3.26 presents the temperature at the end of the process ΔT in comparison to reference temperature T and allows to see a clearer picture of the phenomenon happening in Fig. 3.25. The behavior of the material changes at about 350°C. Up to the temperature of about 350°C the $T - T_0$ depending on the reference temperature increases gradually. After reaching the 350°C threshold, the difference between initial and final temperature starts to decrease. Such phenomenon was observed by the author, and the hypothesis is the following. The author supposes that initially, as the temperature increases, the material's thermo-elastic cooling causes the temperature difference $T - T_0$ to increase. In the selected model, thermo-elastic cooling is temperature dependent in two ways - Eq. (3.2). Firstly, along with rising absolute temperature of the sample, the value of H also increases, but it is also dependent on the elastic parameters of the material, especially on the Young's modulus, which decreases when the temperature increases - Fig. 3.14. At the temperature 350°C = 623.15 K Young's modulus is almost reduced in half. From this moment on, the second effect dominates, which is the decrease of the source of cooling because of the decreasing stiffness of the material.

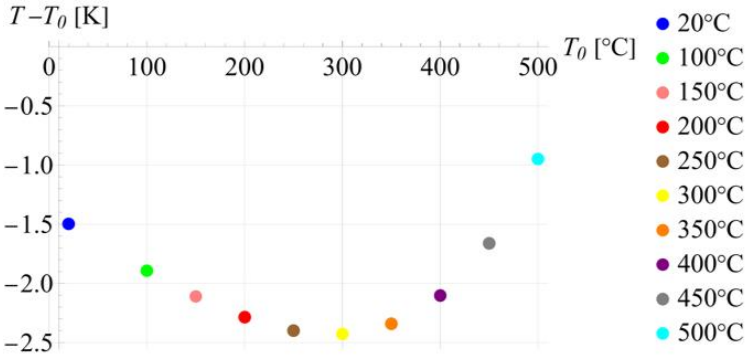

Figure 3.26: Difference between final and initial temperature compared to the reference temperature at the end of the process.

3.5 Convection tests

The objective of the test is to determine whether taking into account the convection phenomenon will influence the results of the simulations in the elastic range. A plate of 100 mm in length (L), 25 mm width

(W) and thickness (H) of 2 mm made out of aluminum alloy AW5083 was applied in the simulation. A visual 3D representation of the plate can be seen below in Fig. 3.27. The shape of the sample models the central part of the Dog-Bone sample from (Mucha et al., 2023).

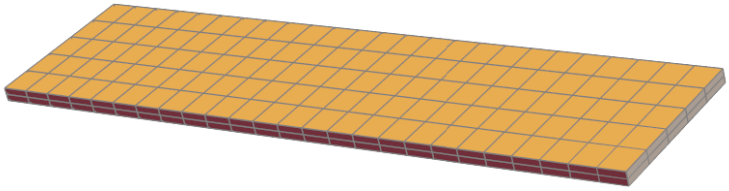

Figure 3.27: Visual representation of the plate used in convection tests.

The time duration of the test was set to 15 s and the elongation was assigned to be $\frac{L}{150}$. From such elongation we can calculate, that the strain rate is then equal to $\dot{\epsilon}_{aver} = 4.4 \times 10^{-4}$ calculated according to the formula

$$\dot{\epsilon}_{aver} = \frac{\epsilon}{t}, \tag{3.18}$$

where t represents time of the process and

$$\epsilon = \frac{\Delta L}{L}, \tag{3.19}$$

ΔL being the elongation of the plate, and L being the initial length of the plate.

Adopting such shape and strain rate allows the conditions to be reproduced as closely as possible to the conditions to which the aluminum sample was subjected in the tests (Mucha et al., 2023). The purpose of the simulation is to check whether convection influences the test results and, if so, to what extent. Material parameters are as shown in Table 2.6. Boundary conditions applied in the simulation were assigned in the following way. The mechanical boundary conditions were set to a fixed support at the beginning of the sample, that is, along the left side of the plate. Such type of support restricts the movement of the sample in all directions. The right side of the plate is clamped, and is connected to the machine which is generating force driving the deformation of the aluminum plate. The clamp acts as a guided support, which means it allows for the movement in the range of one degree of freedom, here horizontal. The thermal boundary conditions were defined as follows: since at the support and between the clamps the heat transfer is limited, the boundary conditions are assumed to be insulation.

A special mesh designated for convection made out of 2D rectangles was also applied. In Fig. 3.28 one can see a visualization of the mesh.

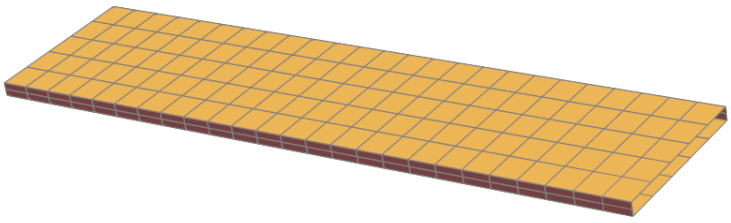

Figure 3.28: Visual representation of the mesh used for convection simulation.

Property	Symbol	Value	Unit
Temperature of surrounding	T_∞	293.15	K
Convection coefficient	h_{conv}	0.1, 10, 100	J/(sKm^2)

Table 3.1: Convection parameters.

Table 3.2 presents more detailed temperature values at selected points in the sample.

Convection coefficient	Point	Temperature value	Unit
$h_{conv} = 0$	Middle	291.799	K
	Surface	291.799	K
	End	291.740	K
$h_{conv} = 1$	Middle	291.803	K
	Surface	291.803	K
	End	291.745	K
$h_{conv} = 10$	Middle	291.844	K
	Surface	291.844	K
	End	291.786	K
$h_{conv} = 100$	Middle	292.171	K
	Surface	292.171	K
	End	292.121	K

Table 3.2: Detailed analysis of temperature values applying different convection parameters.

The term *Middle* refers to the point of the following coordinates: $(L/2, W/2, H/2)$, where symbols L, W and H respectively denote length, width and height of the sample applied in the simulation of the convection test. Secondly, *Surface* refers to the point of coordinates: $(L/2, W/2, H)$ and lastly the term *End* refers to the point: $(L, W/2, H/2)$ near the clamp of the machine.

A special mesh designed to examine whether the density of mesh used for the tests will influence the results, and if so, to what extend. Below one can see visualizations of three meshes used in order to check, whether the density of mesh influences the change in temperature. Note, that mesh refinement was also increasing along the height of the plate by the same multiplication factor as along other dimensions of the plate, but such way of presentation was chosen to maintain clarity of the figures.

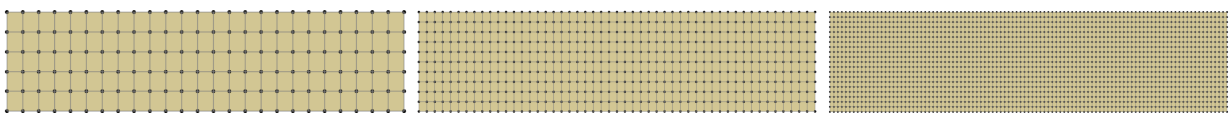

(a) Coarse mesh. (b) Medium mesh. (c) Fine mesh.

Figure 3.29: Visual representation of different mesh refinement used to determine influence of mesh density on temperature change.

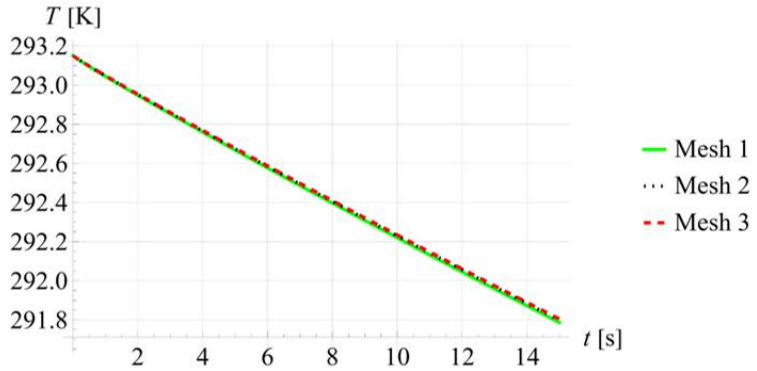

Figure 3.30: Dependence of temperature on the density of mesh for the convection coefficient $h_{conv} = 10$.

The test was carried out for the heat transfer coefficient $h_{conv} = 10$ accordingly to Table 2.2 for all three meshes presented in Fig. 3.29. The results of the test were compared and can be seen in Fig. 3.30. As an outcome of the comparison, the conclusion is that the results are almost independent on the mesh refinement therefore the later presented analysis of the change in temperature for various convection coefficients h_{conv} was conducted with application of the mesh shown in Fig. 3.29a and Fig. 3.28 to optimize the accuracy and efficiency of the simulations. After establishing mesh refinement, test aiming to examine change in temperature depending on the assigned convection coefficient h_{conv} was carried out. The results of the following test can be seen in the next paragraph.

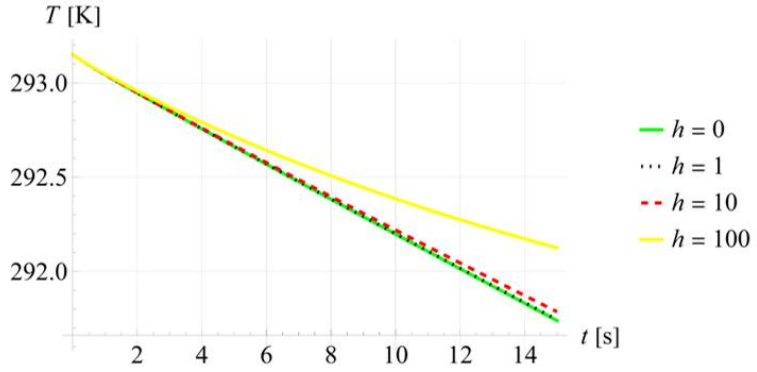

Figure 3.31: Temperature depending on the value of convection coefficient h_{conv}.

From the figure on the right, Fig. 3.31 and after closer examination of the results presented in Table 3.2 it is concluded, that the process of convection does in fact influence the temperature differences, moreover, it influences the way that temperature changes. The higher in value convection coefficient is applied, the more nonlinear form of change in temperature is observed.

Chapter 4

Thermo-elasto-plasticity

4.1 Description of the Thermo-elastic-plastic Model

The yield function F is written in the following form

$$F = f - \sqrt{\frac{2}{3}}\sigma_y \tag{4.1}$$

where f is the Mises stress measure defined as

$$f = \sqrt{\mathbf{s} : \mathbf{s}} \tag{4.2}$$

where

$$\mathbf{s} = \boldsymbol{\tau} - \frac{1}{3}\mathrm{tr}(\boldsymbol{\tau})\mathbf{I} \tag{4.3}$$

and $\boldsymbol{\tau}$ is the Kirchhoff stress tensor (Ristinmaa et al., 2007). The yield strength for the applied thermo-elastic-plastic model is written in the following form

$$\sigma_y = \sigma_{y0} - h \tag{4.4}$$

where the internal hardening variable h has a form

$$h = (\sigma_{y\infty} - \sigma_{y0})(1 - e^{-\delta\alpha}) \tag{4.5}$$

where σ_{y0} is initial yield stress, $\sigma_{y\infty}$ is residual yield stress and δ denotes saturation parameter (Mucha et al., 2023).

$$\sigma_{y0}(T) = 2.8397 \times 10^8 - \frac{2.5154 \times 10^8}{1 + e^{13.769 - 0.0262T}} \tag{4.6}$$

$$\sigma_{y\infty}(T) = 3.5557 \times 10^8 - \frac{3.1924 \times 10^8}{1 + e^{13.827 - 0.027T}} \tag{4.7}$$

The balance of energy has the form

$$c_0\dot{T} = \mathrm{Div}(\mathbf{Q}) - \mathcal{H} - D_{mech} - \mathcal{A} \tag{4.8}$$

The three internal heat source functions present as follows. Function $\mathcal{H}$ representing the elasto-plasto structural heating (Ĉanadija and Brnić, 2004) has a form

$$\mathcal{H} = T\frac{\partial \boldsymbol{\tau}}{\partial T} : [\mathbf{d} - \mathbf{d}^p] \tag{4.9}$$

where $\mathbf{d}^p$ is the plastic part of the symmetric velocity gradient. The mechanical dissipation presents then as

$$D_{mech} = \boldsymbol{\tau} : \mathbf{d}^p - h\alpha \tag{4.10}$$

and the function $\mathcal{A}$ which describes the temperature dependence of the thermodynamic force correlated to the hardening variable looks as follows

$$\mathcal{A} = T\frac{\partial h}{\partial T}\dot{\alpha} \tag{4.11}$$

4.2 Results for 1FE

A test for one finite element was conducted. A cube of dimensions $L = 10$ mm, $W = 10$ mm, $H = 10$ mm was subjected to elongation equal $\Delta L = \frac{L}{4}$. Visual representation of the finite element (FE) in three dimensional space (3D) can be seen in Fig. 4.1. Such elongation allowed to test the sample taking into consideration also plastic range of deformations. In Figs. 4.2 - 4.5 the author compares how the function of temperature and reactions change when setting different test time t.

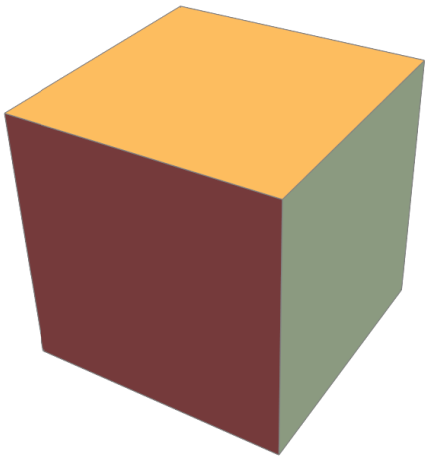

Figure 4.1: Visual representation of 1 FE in 3D.

Such elongation allowed to test the sample taking into consideration also plastic range of deformations. Below the author compares how temperature of the aluminum sample changes when setting different test time t.

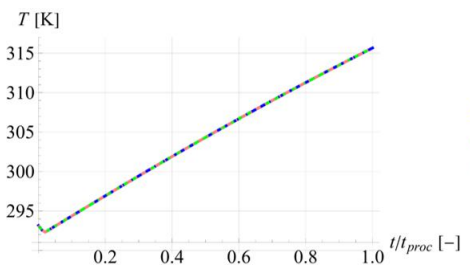

Figure 4.2: Temperature change depending on test time.

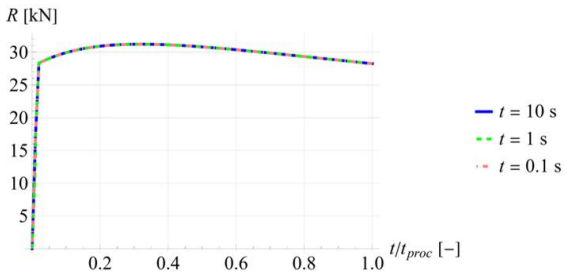

Figure 4.3: Change in magnitude of reactions depending on test time.

It is apparent from Fig. 4.2 and Fig. 4.3 that the testing time does not influence the way temperature of the sample or the magnitude of reactions changes. It is very well seen when the elastic range of deformations ends, and the plastic one begins. A plastic shelf forms, and the material's sample enters the range of

irreversible deformations. In terms of temperature change, the sample undergoes elastic cooling at the beginning, and then as expected, starts to rapidly increase its temperature with further deformations.

Results presented previously in Fig. 4.2 and Fig. 4.3 were obtained by computing tests with material's parameters depending on temperature T_0 and for initial temperature equal to 293.15 K. Below the author presents graphs of the change in temperature depending on test time and the change in magnitude of reactions depending on assigned test time for fixed material's parameters.

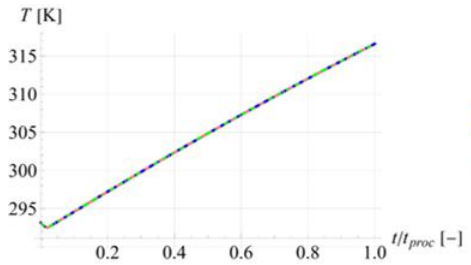

Figure 4.4: Temperature change depending on test time for fixed parameters.

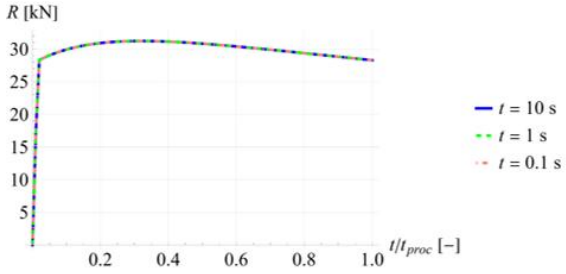

Figure 4.5: Change in magnitude of reactions depending on test time for fixed parameters.

After examination of test results for material's parameters dependent on the reference temperature and tests performed for fixed material's parameters, the difference might not be apparent from the graphs only. For that reason, the author examined the results closer, and concluded that the maximum magnitude of the reactions is indeed the same for both cases and equals $R = 31.2$ kN. A change in test results is significant at the end of the process. In case of tests with material's parameters dependent on temperature, the magnitude of reactions at the end of the process equals $R = 28.2$ kN, however in case of test results with fixed material's parameters, R at the end of the process equals $R = 28.3$ kN.

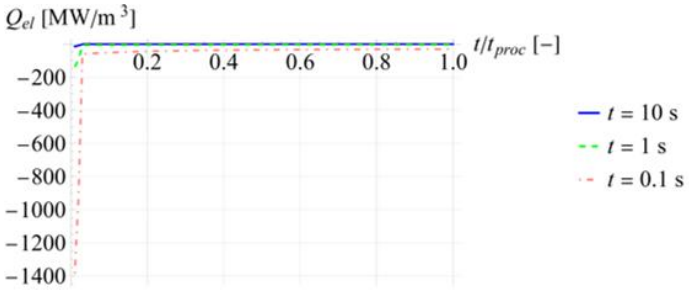

Figure 4.6: Elastic heating.

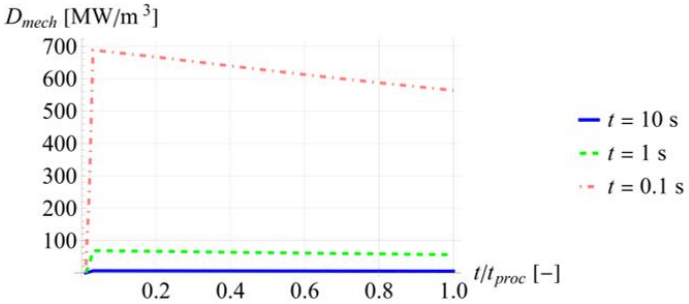

Figure 4.7: Mechanical energy dissipation.

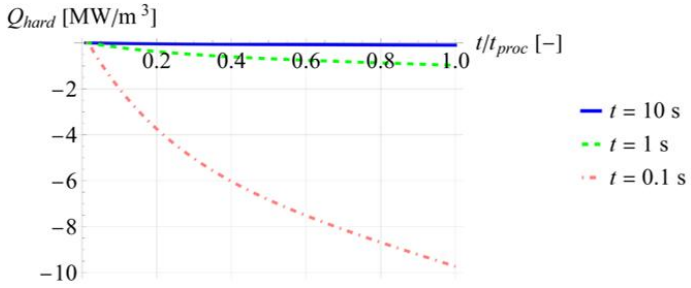

Figure 4.8: Heat generation due to hardening.

All three energy sources which were analyzed and the results of the analysis are present in Figs. 4.6 - 4.8 show a trend suggesting energy dissipation within the system. The initial large difference in the value of mechanical energy dissipation D_{mech} visible in Fig. 4.7 for timescale $t = 0.1$ s suggests a rapid initial energy release. The rapid initial decrease and subsequent slower decay of Q_{hard} value seen in Fig. 4.8 could be attributed to the conversion of energy to heat and resistive losses. The shorter the time of the process, the faster the heat gets transferred away from the source.

Because the model does not include viscosity phenomena, which might be present when testing the sample in 0.1 s, process time $t = 10$ s is applied for further testing.

Based on Fig. 2.8 the author prepared a graph presenting the relationship between engineering stress and change in the length of the sample, which can be seen in Fig. 4.9. The serrations are omitted in the simulation thus in Fig. 4.9 they are also omitted.

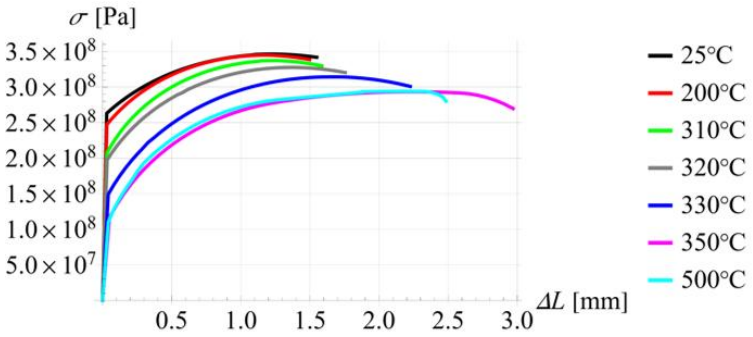

Figure 4.9: Engineering stress vs. change in length of the sample.

Similarly as in Section 3.4 an analysis of the influence of the initial temperature on how the temperature function changes throughout the process was conducted. The result of the analysis can be seen in Fig. 4.10. The sample heats up to the extend, that the temperature evolution can be seen with a naked eye. The phenomenon is further investigated and the results are present in Figs. 4.12 and 4.13.

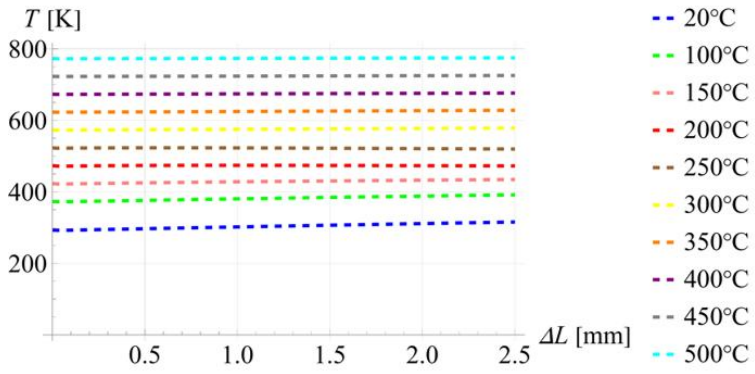

Figure 4.10: Dependence of temperature on reference temperature.

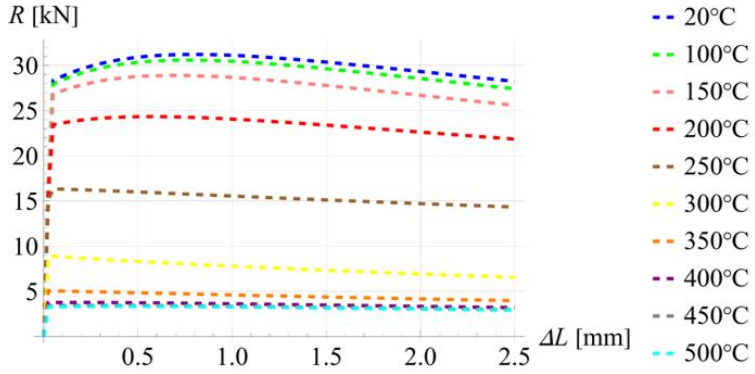

Figure 4.11: Dependence of reactions on reference temperature.

With an increase in the reference temperature, the reactions of the sample progressively decrease, which can be seen in Fig. 4.11. At the very beginning an almost linear phase is present on the graph, then the material hardens, therefore an ideal plastic shelf is not formed. Instead, after hardening of the material, a phase of softening begins. In Fig. 4.12 as well as in Fig. 4.13 one can see that the difference between initial temperature T_0 and temperature at the end of the process T is strongly dependent on initial temperature. The author assumes the reason for such behavior of the material is how the material's yield threshold changes with temperature which is presented in Figs. 3.19 and 3.20. At about 250°C = 523.15 K the plastic limit changes, therefore causing the material to heat up less during the process, which directly leads to the difference between T and T_0 becoming smaller.

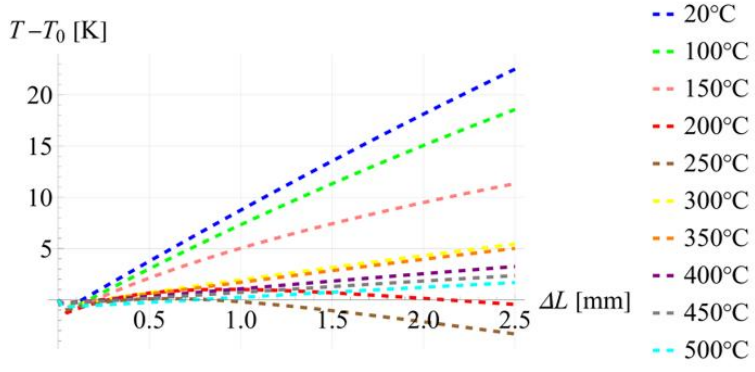

Figure 4.12: Dependence of the difference between final and initial temperature on reference temperature.

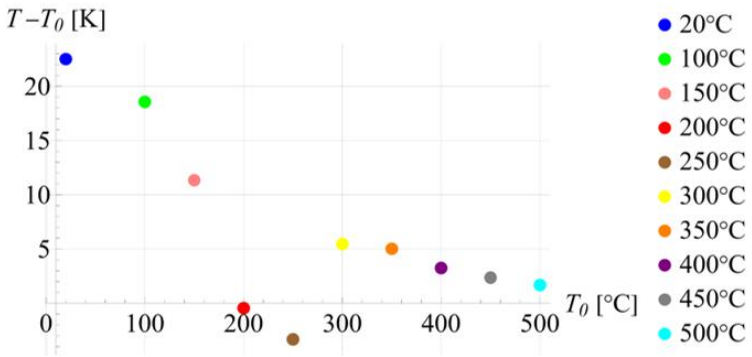

Figure 4.13: Dependence of the difference between final and initial temperature on reference temperature at the end of the process.

4.3 Results for the Dog-Bone sample

4.3.1 Dog-Bone sample

To best model the testing conditions from the tests performed and described in the work (Mucha et al., 2023), a dog-bone-shaped sample was introduced. The shape and dimensions of the sample can be seen in Fig. 4.14. The thickness of the specimen is $H = 2$ mm. The sample was subjected to elongation of $\Delta L = \frac{L}{4}$ in time duration of $t = 10$ s. In Fig. 4.14, one can see the shape of the sample with the dimensions expressed in mm. All tests done for the Dog-Bone shaped sample were performed for temperature dependent material parameters.

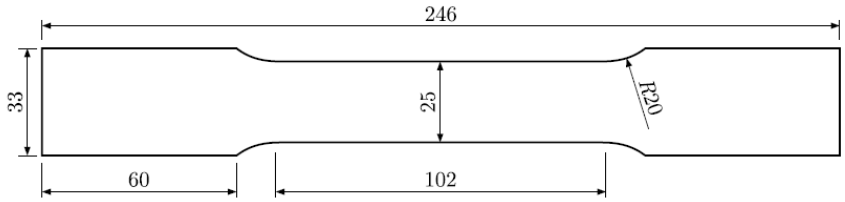

Figure 4.14: Sample shape and dimensions given in mm (Wcisło et al., 2024).

To ensure the most numerically accurate results, a room temperature test was performed - $T_0 = 293.15$ K in time $t = 10$ s for meshes of three densities. In Fig. 4.15 one can find visual representation of the three meshes used for the test. Insulation conditions were assumed - $h_{conv} = 0$.

(a) Coarse mesh. (b) Medium mesh. (c) Fine mesh.

Figure 4.15: Visual representation of different mesh refinement used to determine influence of mesh density on temperature change.

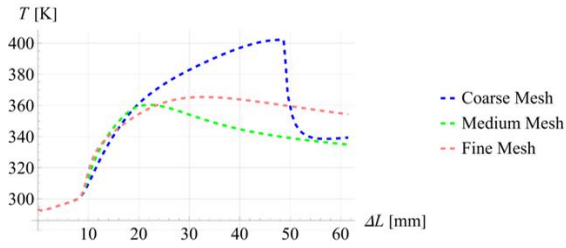

Figure 4.16: Temperature depending on the refinement of the mesh in mid point of the sample.

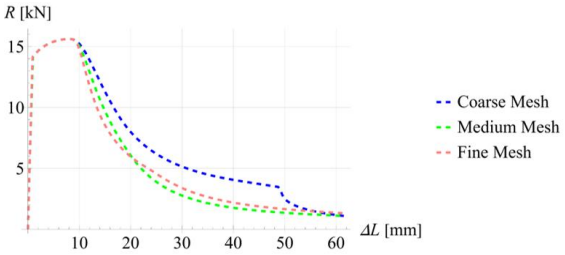

Figure 4.17: Reactions depending on the mesh refinement in mid point of the sample.

The conclusion from the comparison seen in Fig. 4.16 and Fig. 4.17 is as follows. For the the thermo-elastic range the results for all three meshes taken into consideration are consistent. Such a conclusion is persistent with the outcome of the mesh analysis presented in Subsection 3.3.3 for the range of reversible deformations. The same conclusion can be made for the plastic range of material hardening which takes place until about $\Delta L = 10$ mm. After material hardening the results for different meshes stop being consistent with each other. The medium mesh was chosen for the remaining tests to keep the efficiency of the testing process without a great effect on the numerical accuracy of the results.

4.3.2 Convection

The conclusions made from the previous chapter were the basis to testing how the thermo-elasto-plastic model is going to be influenced by the convection phenomenon. Similarly as in thermo-elastic analysis, a special mesh is implemented allowing for more advanced analysis of the thermal boundary conditions. The mechanical boundary conditions are determined to a fixed support at $L = 0$ mm. Such type of support restricts the movement of the sample in all directions. The right side of the plate is clamped, and is connected to the machine which is generating force driving the deformation of the aluminum plate. The clamp acts as a guided support, which means it allows for the movement in the range of one degree of freedom, here horizontal. The thermal boundary conditions were defined as follows: since at the support and between the clamps the heat transfer is limited, the boundary conditions are assumed to be $h_{conv} = 0$.

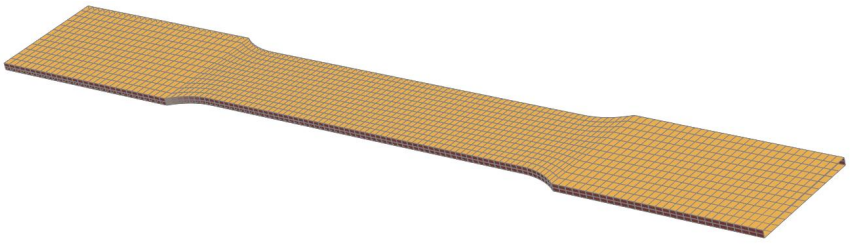

Figure 4.18: 3D visual representation of the mesh used for convection analysis for the Dog-Bone sample.

Property	Symbol	Value	Unit
Temperature of surrounding	T_∞	293.15	K
Convection coefficient	h_{conv}	10, 100	J/(sKm^2)

Table 4.1: Convection parameters.

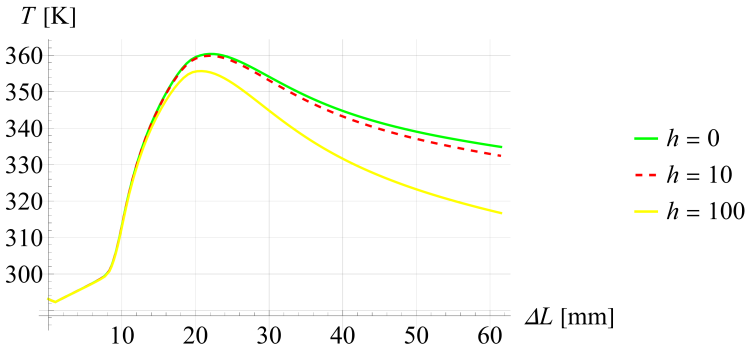

Figure 4.19: Temperature difference depending on the value of convection coefficient h_{conv}.

Analogically as in Fig. 4.16 and Fig. 4.17 the results for all convection coefficients h_{conv} taken into consideration in the range of reversible deformations and material hardening range are very close. With bigger convection coefficient the difference between initial temperature and temperature at the end of the test becomes smaller. For the remaining tests convection coefficient $h_{conv} = 10$ was chosen.

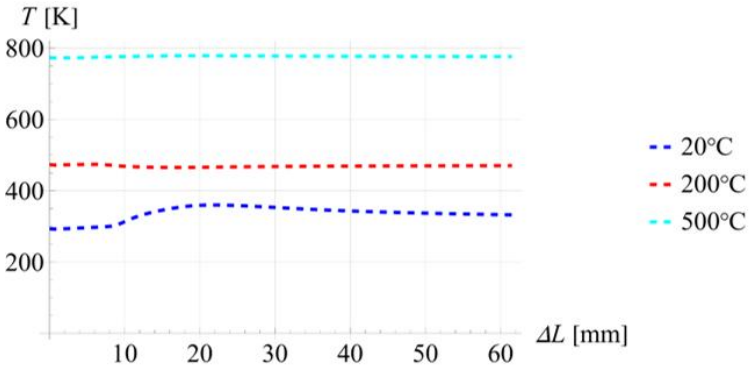

Figure 4.20: Dependence of change in temperature on the reference temperature.

Fig. 4.20 shows temperature function with respect to elongation of the sample ΔL depending on the reference temperature. The biggest amplitude can be observed for the reference temperature $T_0 = 20°C$ which is similar to the results from Fig. 4.10. In Figs. 4.21 - 4.23 a similar analysis as in previous sections was made for reactions and difference between final and initial temperature respectively.

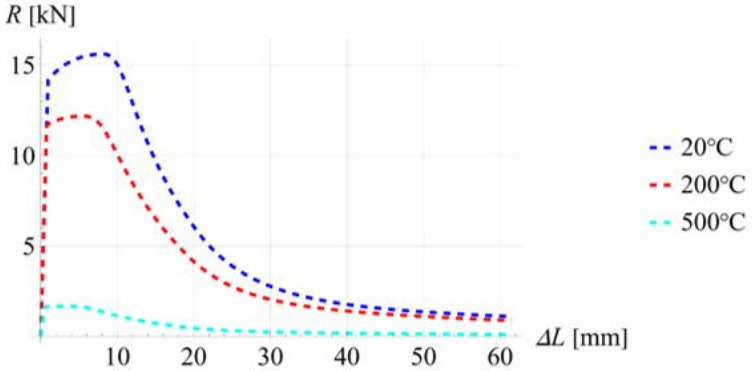

Figure 4.21: Dependence of change in the magnitude of reactions depending on the reference temperature.

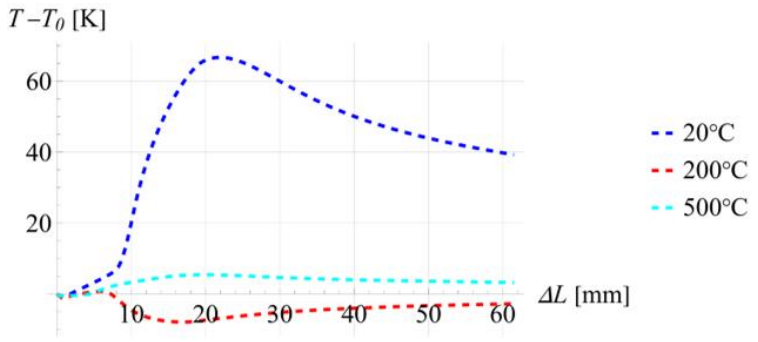

Figure 4.22: Dependence of the difference between final and initial temperature on reference temperature.

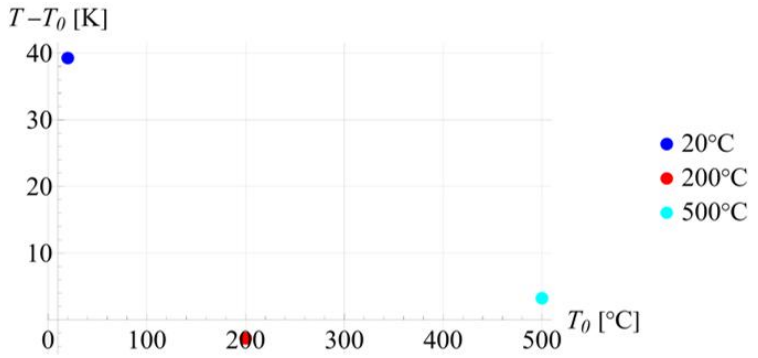

Figure 4.23: Dependence of the difference between final and initial temperature on reference temperature at the end of the process.

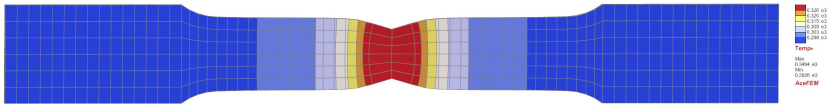

Figure 4.24: Deformed sample with coarse mesh.

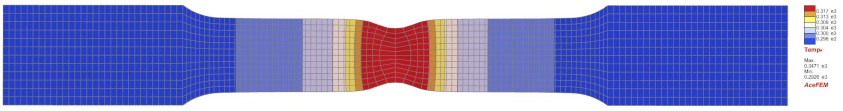

Figure 4.25: Deformed sample with medium mesh.

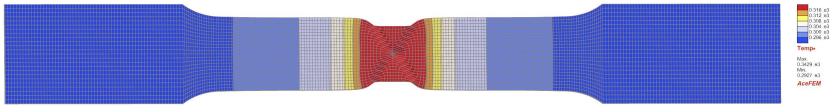

Figure 4.26: Deformed sample with fine mesh.

From Figs. 4.24 - 4.26 one can see that the point of highest temperature is located centrally. For the fine mesh the deformation takes an X shape, which is also true for experimental results (Mucha et al., 2023). Because the results presented in Fig. 4.20 and 4.21 are only valid until about 35 mm of elongation due to the fact that after this point a physical sample would rapture, deformed samples seen in Figs. 4.24 - 4.26 are shown for elongation equal $\Delta L = 30$ mm.

Chapter 5

Conclusions

The objective of the thesis was to develop a model simulating real behavior of an aluminum sample made out of AA5083. The model had to take into account thermo-elastic and thermo-elasto-plastic ranges of deformations. The goal of the thesis was achieved by application of numerical simulation packages AceGen and AceFEM from Wolfram Mathematica toolbox.

Chapter 2 introduced most fundamental concepts for kinematics, heat transfer, thermal expansion and plastic dissipation, which were then implemented in numerical simulation models.

In Chapter 3 several tests for one finite element were conducted for reversible large-strain deformations. The first analyzed aspect was the influence of the form of the volumetric part of the Helmholtz free energy which was applied on the results for 1FE simulations. After performing tests for a cube element, tests for more complex samples were completed. An analysis of a rectangular plate in non-uniform tension as well as analysis of convection process for a thin plate simulating the central part of a Dog-Bone sample have been described. The author analyzed the influence of the temperature at the beginning of the process with consideration of temperature dependent parameters.

In Chapter 4 several tests have been performed for 1FE as well as for a Dog-Bone shaped sample. Plastic deformations were tested for constant and temperature dependent material parameters. The influence of convection process was also a subject of analysis interposed in this chapter. The implementation of thermo-elastic coupling phenomenon to the thermo-elasto-plastic model allows one to notice where the reversible deformations end and irreversible deformations begin. Presented approach successfully solves problems generated from isochoric behavior of irreversible deformations.

Results obtained in numerical simulations show good correlation with existing experimental results. From the results presented in the work it is concluded that the model properly simulates true behavior of the material. The model does not take into account viscous effects, which can be considered for further, more advanced part of the research.

Bibliography

Albatici, R., Passerini, F., Tonelli, A., and Gialanella, S. (2013). Assessment of the thermal emissivity value of building materials using an infrared thermovision technique emissometer. *Energy and Buildings*, 66:33–40.

Bahrami, M. (2011). Transient conduction heat transfer. Laboratoy for Alternative Energy Conversion.

Belytschko, T., Moran, B., and Kulkarni, M. (1991). On the crucial role of imperfections in quasi-static viscoplastic solutions. *Journal of Applied Mechanics*, 58:658–665.

Bonet, J. and Wood, R. D. (2008). *Nonlinear continuum mechanics for finite element analysis*. Cambridge University Press, Cambridge, second edition.

Ĉanadija, M. and Brnić, J. (2004). Associative coupled thermoplasticity at finite strain with temperature-dependent material parameters. *Int. J. Plasticity*, 20:1851–1874.

CEN (2002). Eurocode 1: Actions on structures - part 1-2: General actions - actions on structures exposed to fire. Technical report, European Committee for Standardization (CEN). EN 1991-1-2:2002, Section 3.3.

CEN (2005). Eurocode 9: Design of steel structures. Technical report, European Committee for Standardization (CEN). EN 1999-1-1:2007.

Chiavazzo, E., Ventola, L., Calignano, F., Manfredi, D., and Asinari, P. (2014). A sensor for direct measurement of small convective heat fluxes: Validation and application to micro-structured surfaces. *Experimental Thermal and Fluid Science*, 55:42–53.

Churchill, S. W. and Chu, H. H. (1975). Correlating equations for laminar and turbulent free convection from a vertical plate. *International Journal of Heat and Mass Transfer*, 18(11):1323–1329.

Clifton, R. J., Duffy, J., Hartley, K. A., and Shawki, T. G. (1984). On critical conditions for shear band formation at high strain rates. *Scripta Metallurgica*, 18(5):443–448.

Elsayed, M., Shash, A., Mahmoud, T., and Rabbou, M. (2017). Effect of friction stir welding parameters on the peak temperature and the mechanical properties of aluminum alloy 5083-o. *Advanced Structured Materials*, pages 11–25.

EngineersEdge (n.d.). Convective heat transfer coefficients table. Accessed: 2025-01-20.

Farren, W. S. and Taylor, G. I. (1925). The heat developed during plastic extension of metals. *Proceedings of the Royal Society of London. Series A, Containing Papers of a Mathematical and Physical Character*, 107(743):422–451.

Gough, J. (1805). A description of some curious phenomena discovered in the twisting of glass rods. *Memoirs of the Literary and Philosophical Society of Manchester*, 3:288–295.

Haupt, P. (2002). *Continuum Mechanics and Theory of Materials*. Springer.

Holman, J. P. and Churchill, S. W. (1999). Incident radiation and its effects on solar cells. *Solar Energy Materials & Solar Cells*, 56(1):1–20.

Holzapfel, G. A. (2000). *Nonlinear Solid Mechanics. A Continuum Approach for Engineering*. John Wiley & Sons, Chichester.

Humphreys, J. F. and Parsons, A. (2002). Thermal comfort in buildings: A review. *Building Services Engineering Research & Technology*.

Incropera, F., DeWitt, D., Bergman, T., and Lavine, A. (2007). *Fundamentals of Heat and Mass Transfer*. John Wiley & Sons, Inc.

Incropera, F. P., DeWitt, D. P., Bergman, T. L., and Lavine, A. S. (2017). *Principles of Heat and Mass Transfer*. Wiley, Hoboken, NJ, USA, 8th edition.

Korelc, J. (2009). Automation of primal and sensitivity analysis of transient coupled problems. *Computational Mechanics*, 44:631–649.

Korelc, J. and Wriggers, P. (2016). *Automation of Finite Element Methods*. Springer International Publishing Switzerland.

Lee, E. H. and Liu, D. T. (1968). Finite strain elastic-plastic theory. In Parkus, H. and Sedov, L. I., editors, *Irreversible Aspects of Continuum Mechanics and Transfer of Physical Characteristics in Moving Fluids*, pages 213–222, Vienna. Springer Vienna.

Lu, S. C. H. and Pister, K. S. (1975). Decomposition of deformation and representation of the free energy function for isotropic thermoelastic solids. *Int. J. Solids Struct.*, 11:927–934.

Miehe, C. (1995). Entropic thermoelasticity at finite strains. aspects of the formulation and numerical implementation. *Comput. Methods Appl. Mech. Engrg.*, 120:243–269.

Mohamed, A.-M. O. and Paleologos, E. K. (2018). Chapter 9 - subsurface contaminant transport. In Mohamed, A.-M. O. and Paleologos, E. K., editors, *Fundamentals of Geoenvironmental Engineering*, pages 283–324. Butterworth-Heinemann.

Mucha, M., Rose, L., Wcisło, B., Menzel, M., and Pamin, J. (2023). Experiments and numerical simulations of lueders bands and portevin–le chatelier effect in aluminium alloy aw5083. *Arch. Mech.*

Planck, M. (1901). Über die theorie des gesetzes der schwarzen strahlung. *Verhandlungen der Deutschen Physikalischen Gesellschaft*, 3(17):457–463.

ResearchGate, C. (n.d.). How much heat transfer coefficient of air? Accessed: 2025-01-20.

Ristinmaa, M., Wallin, M., and Ottosen, N. S. (2007). Thermodynamic format and heat generation of isotropic hardening plasticity. *Acta Mechanica*, 194:103–121.

Roberts, R. B. and Kirkwood, J. L. (1940). Thermal expansion of solids: A review. *The Review of Modern Physics*.

Simo, J. C. and Miehe, C. (1992). Associative coupled thermoplasticity at finite strains: Formulation, numerical analysis and implementation. *Comput. Methods Appl. Mech. Engrg.*, 98(1):41–104.

Sokolova, I. (2019). Temperature regulation. In Fath, B., editor, *Encyclopedia of Ecology (Second Edition)*, pages 633–639. Elsevier, Oxford, second edition edition.

Stojanović, R., Djurić, S., and Vujošević, L. (1964). On finite thermal deformations. *Arch. Mech. Stos.*, 16:103–108.

Summers, P., Chen, Y., Rippe, C., Allen, B., Mouritz, A., Case, S. W., and Lattimer, B. (2015). Overview of aluminum alloy mechanical properties during and after fires. *Fire Science Reviews*, 4.

Sun, S. and Zhang, T. (2020). Chapter two - review of classical reservoir simulation. In Sun, S. and Zhang, T., editors, *Reservoir Simulations*, pages 23–86. Gulf Professional Publishing.

Taylor, G. I. and Quinney, H. (1934). The latent energy remaining in a metal after cold working. *Proceedings of the Royal Society of London. Series A, Containing Papers of a Mathematical and Physical Character*, 143:307–326.

Wcisło, B., Mucha, M., and Pamin, J. (2024). Internal heat sources in large strain thermo-elasto-plasticity - theory and finite element simulations. *Journal of theoretical and applied mechanics*, 62:293–306.

Yang, H., Sinha, S. K., Feng, Y., McCallen, D. B., and Jeremić, B. (2017). Energy dissipation analysis of elastic–plastic materials. *Computational Mechanics*, 61:591–602.

Çengel, Y. A. and Ghajar, A. J. (2014). *Heat and Mass Transfer: Fundamentals & Applications*. McGraw-Hill Education, 5th edition.